Title
The Small Conserved CM2 Domain in Centrosomin is a Multi-functional Binding Domain that Drives Protein Organization in the Centrosome

Author
Citron, Yemima Rose

Publication Date
2018

Peer reviewed|Thesis/dissertation

The Small Conserved CM2 Domain in Centrosomin is a Multi-functional Binding Domain that Drives Protein Organization in the Centrosome

by

Yemima Rose Citron

DISSERTATION

Submitted in partial satisfaction of the requirements for the degree of

DOCTOR OF PHILOSOPHY

in

Biophysics

in the

GRADUATE DIVISION

of the

UNIVERSITY OF CALIFORNIA, SAN FRANCISCO

Acknowledgements

I'd like to acknowledge the guidance, patience and support of David Agard and Bo Huang throughout my PhD. For scientific help on my thesis work, I'd like to thank the following people: James Holton for immense efforts in phasing crystal diffraction data. Mark Kelly for his endless guidance and help learning NMR and beyond; Daniel Elnatan for help with SAXS data collection and processing; Ryan McGorty for his incredible expertise on optical microscopes; Wei Qiang Ong and Veronica Pessino for help with FACS.

Overall, I'd like to thank various members of the Agard lab past and present who have been a source of guidance and friendship; James Kraemer, Laura Lavery, Elaine Kirschke, Rebeca Choy, Ray Wang, Mariano Tabios, Kliment Verba (Klim Klam), Daniel Elnatan, and in particular Andrew Lyon and Miguel Betegon-Ramiro whose passionate conversation makes me feel better in this world.

Outside the UCSF community, I'd like to thank: the Maas family who has adopted me as their own and specifically my close friend, Lavit Maas; my cousins the Chezars and specifically Judy Chezar who is an incredible scientist and human; my wonderful family, Tamar King, Rafi Citron, Zvi Citron, Shira Citron, Tzippy Citron and all the littlest Citrons, Zohar, Amalia, and baby Aloe.

Finally, but foremost, my father Richard Citron, to whom this thesis is dedicated. His compassion, wit and intellect are missed in this world.

The Small Conserved CM2 Domain in Centrosomin is a Multi-functional Binding Domain that Drives Protein Organization in the Centrosome

by

Yemima Rose Citron

Abstract

The centrosome serves as the main microtubule-organizing center in metazoan cells, yet despite its functional importance, little is known mechanistically about the structure and organizational principles that dictate protein organization in the centrosome. In particular, the protein-protein interactions that allow for the massive structural transition between the tightly organized interphase centrosome and the highly expanded matrix-like arrangement of the mitotic centrosome have been largely uncharacterized. Among the proteins that undergo a major transition is the *Drosophila melanogaster* protein centrosomin that contains a conserved carboxyl terminus motif, CM2. Recent crystal structures have shown this motif to be dimeric and capable of forming an intramolecular interaction with a central region of centrosomin. Here we use a combination of in-cell microscopy and *in vitro* oligomer assessment to show that dimerization is not necessary for CM2 recruitment to the centrosome and that CM2 alone undergoes significant cell cycle dependent rearrangement. We use NMR binding assays to confirm this intramolecular interaction and show that residues involved in solution are consistent with the published crystal structure and identify L1137 as critical for binding. Additionally, we show for the first time an *in vitro* interaction of CM2 with the *Drosophila* pericentrin-like-protein that exploits the same set of residues as the intramolecular interaction. Furthermore,

NMR experiments reveal a calcium sensitive interaction between CM2 and calmodulin. Although unexpected because of sequence divergence, this suggests that centrosomin-mediated assemblies, like the mammalian pericentrin, may be calcium regulated. From these results, we suggest an expanded model where during interphase CM2 interacts with pericentrin-like-protein to form a layer of centrosomin around the centriole wall and that at the onset of mitosis this population acts as a nucleation site of intramolecular centrosomin interactions that support the expansion into the metaphase matrix.

Table of Contents

List of Figures

Chapter I - Introduction

Chapter II- The centrosomin CM2 domain is a multifunctional binding domain with distinct cell cycle roles.

Chapter III – Characterization of CM2 dimerization and the multiple species of dimeric CM2.

Chapter IV – X-Ray Crystallography and Structural Studies of CM2

Chapter I – Introduction

The centrosome is the main microtubule organizing center is metazoan cells and has a number of roles from ensuring the fidelity of mitosis to templating the axoneme of ciliated cells to establishing polarity in asymmetric division. It was first described over a hundred years ago in 1883 by Edouard Van Beneden and in 1888 by Theodor Boveri who carried out a series of experiments in sea urchin embryos complete with precise illustrations of the centrosome [1]. Despite over 130 years of experimentation and its known role in cellular processes, a thorough understanding of the centrosome and, in particular, the principles of protein organization and regulation in the centrosome have been elusive. The experiments described in chapter II and III of this thesis are a small part in this century old pursuit of describing the molecular details of the centrosome with the hopes of elucidating more generally the molecular mechanisms harnessed by the centrosome.

From its first description in the 1880s, it was known that the centrosome played a large role in cell division and by the 1960s it was understood that centrosome was linked to microtubule organization [2]. Numerous studies starting in the 1950s [3] used electron microscopy to begin to shed light on the complex macrostructure of the centrosome. From these work in the 1950-1960s it became clear that the centrosome is made up of two microtubulin based structures known as centrioles that vary from 200-400nm in varies species but maintain a nine-fold symmetry. The centrioles are then surrounded by a region known as the pericentriolar material (PCM) from which microtubules are nucleated (Fig 1A) and which expands dramatically upon entry into mitosis in order to increase microtubule nucleation. Embedded into PCM is the γtubulin ring complex which is responsible for nucleating microtubules. Studies have yielded high resolution structures of the γtubulin ring complex allowing for a detailed

understanding of the mechanisms of microtubule nucleation [4]. And yet despite all this work, the electron dense nature PCM, has remained a mystery with little more insight into its underlying architecture revealed by electron microscopy or cryo-tomography (Fig 1B). The level of understating of the PCM structure has remained as an "amorphous cloud" in the literature.

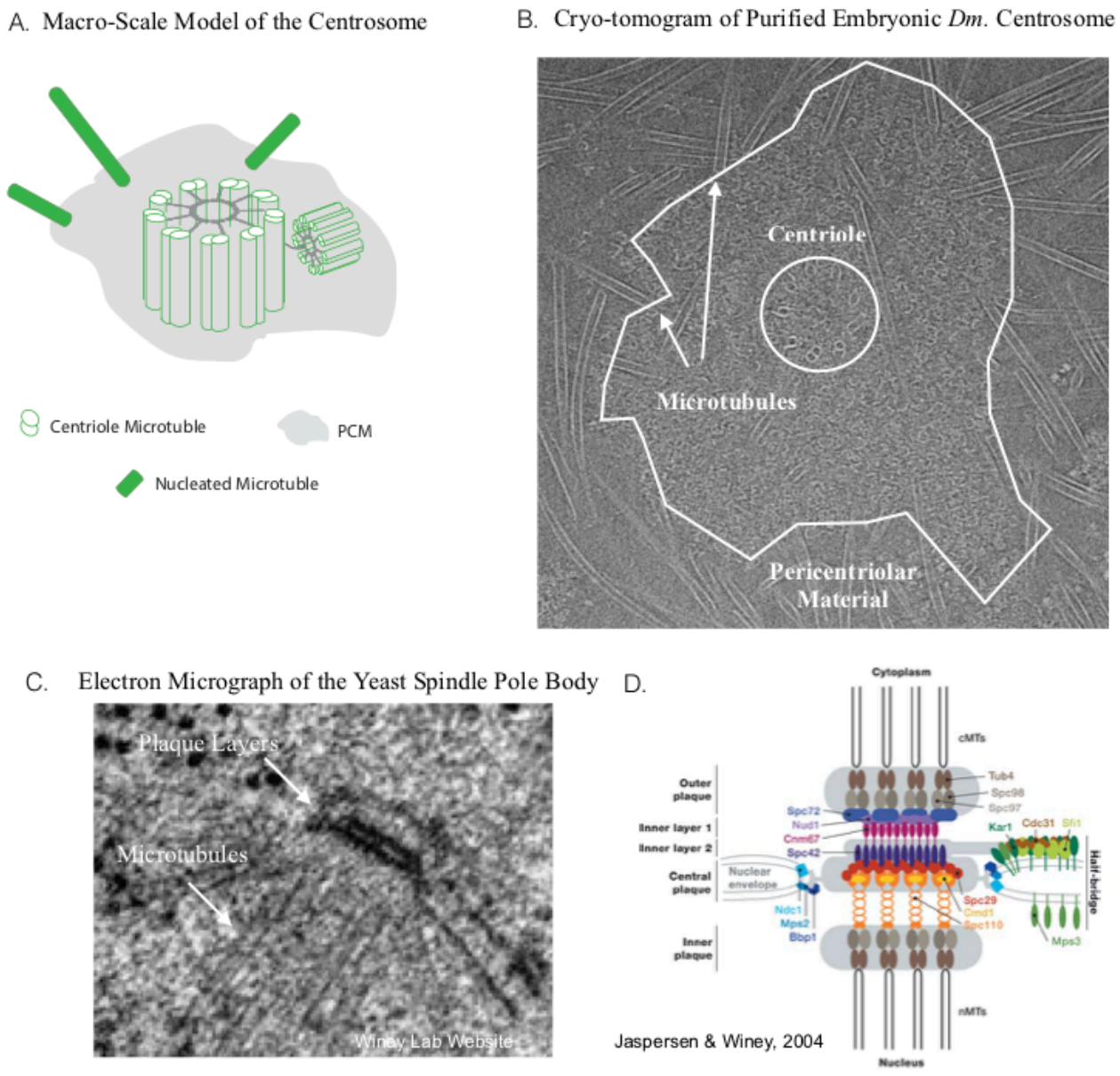

Fig 1. Models and electron microscopy of centrosome and spindle pole body illustrate their basic macrostructure. (A) Schematic of the centrosome showing the microtubulin based mother

and daughter centriole surrounded by the pericentriole material from which microtubules nucleate. (B) A cryo-tomogram of a centrosome purified from drosophila embryos with microtubules regrown post purification. Key features of the centrosome – the centriole, PCM and the nucleated microtubules are highlighted. These data are unpublished work from the Agard lab member Garrett Greenan. (C) An electron micrograph of the yeast spindle pole body (from the Winey lab website: https://winey.faculty.ucdavis.edu) with nuclear microtubules indicated and plaque layers visible. (D) Schematic of the spindle pole body protein organization making up 2D layers of plaque [4].

This basic macrostructure of the centrosome, and the specifically the PCM, is in stark contrast the organization of the spindle pole body (SPB), the functional equivalent of the centrosome in fungi. The SPB is embedded within the nuclear envelope and composed of a two-dimensional plaque upon which layers of protein built upon [5] and can be seen by electron microscopy (Fig 1C). The centrosome's PCM, on the other hand, appears featureless by electron microscopy. Given that both the SPD and the centrosome serve as anchor points to spatially and temporally regulate microtubule nucleation, these profoundly different schemes of protein organization, raises a number of questions. How the centrosome is assembled in interphase? How does the PCM expand during mitosis? How are these processes regulated? What are the advantages of this system of protein organization over the method used in the SPD?

Despite electron microscopy's limitation in elucidating the centrosome ultra-structure, advancements in optical microscopy as well as proteomics and biochemistry have contributed a large body of knowledge about the centrosome. Extensive work isolating centrosomes and preforming mass spectroscopy have identified hundreds of proteins in the centrosome [6,7]. Interestingly, bioinformatics analysis of these proteins has revealed that centrosomal proteins are enriched for predicted coiled-coils regions, intrinsically disordered regions and phosphorylation sites [8] hinting at a general molecular mechanism in the centrosome that utilizes these motifs. Furthermore, genetic interaction studies coupled with optical microscopy have annotated many

of these proteins as either important for centrosome duplication or for centrosome structure as measured by proper distribution of the γtubulin ring complex [9].

Even though, there have been significant advancements in centrosome knowledge, the PCM has still been challenging to study. The resolution limit of traditional wide-field optical microscopy precludes detecting finer detail of these PCM proteins distribution in the centrosome. From a biochemistry approach, numerous studies have attempted to purify, fractionate centrosomes, in order to detect sub-complexes as a means of elucidating the steps of protein assembly required for centrosome formation. These studies have mostly been unable to convincingly observe sub-complexes and have been somewhat inconsistent between techniques, model systems, and laboratories [10,11].

PCM Protein Distributions

The core set of proteins required for unaltered γtubulin ring complex recruitment in drosophila melanogaster is asterless (Asl), pericentrin-like protein (Plp), Sas-4, Spd2, Polo kinase, and centrosomin (Cnn). Studies employing super-resolution optical microscopy and in particular structured illumination microscopy have shed light on a level of substructure previously unseen [12-14]. In interphase Asl, Plp, Sas-4, Spd2, Cnn and γtubulin form rings of various radial distributions around the centriole wall, however, upon entrance into mitosis Spd2, Cnn and γtubulin expand outward creating the matrix of PCM (Fig 2A). These imaging experiments were performed with antibodies targeting various regions of protein allowing for even more detailed conclusions about protein orientation and length to be measured. These data allow us to begin to build a model of protein organization with Sas-4 positioned closest to the centriole wall while Asl and Plp are positioned with their carboxyl termini close to centriole and

their amino termini extended as much as 60nm outward from their carboxyl termini. These arrangements do not change during mitosis. During interphase, Cnn and γtubulin also appear as toroids around the centriole, however, the molecular details of these proteins are much less clear during mitosis.

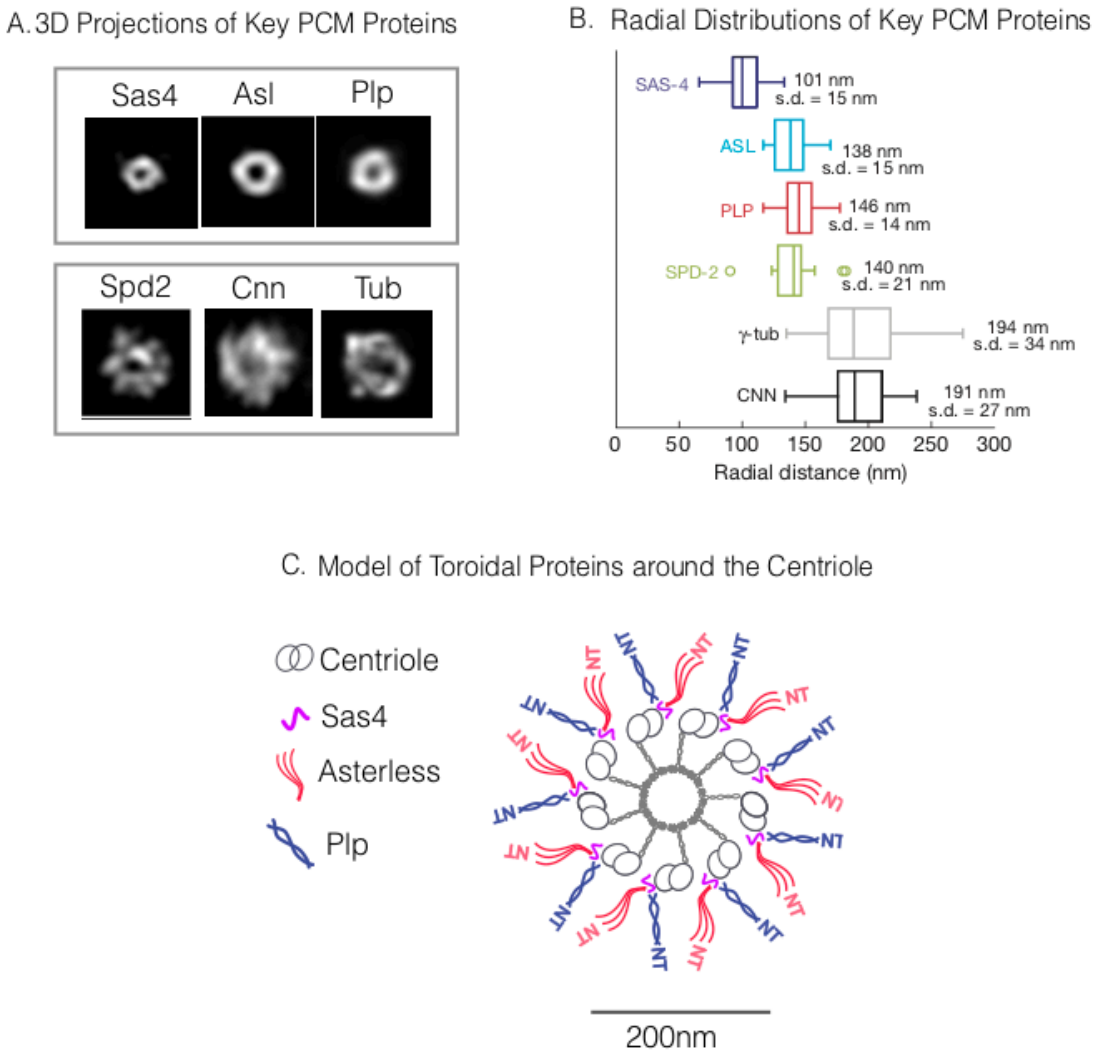

Fig 2. SIM 3D projections and quantifications as a basis for molecular model of the centrosome. (A) 3D projections of PCM proteins acquired by SIM imaging of antibody labeled proteins during mitosis. A tight toroidal distribution can be seen with Sas4, Asl, and Plp. The PCM matrix is formed by the heterogeneous Spd2, Cnn and γtubulin. (B) Quantification of SIM data shows precise measurements of radial distributions for different components. (C) A model of how Sas4, Plp, and Asl are arranged around the centriole wall.

Importantly, each of these proteins is conserved with known human homologues and similar results have been observed via SIM imaging of these proteins suggesting that the principle of centrosome molecular assembly and regulation is also conserved.

Centrosomin and its homologues

Of particular interest, is the protein centrosomin which undergoes a large transition from a toroidal distribution at interphase into a matrix during mitosis. Centrosomin is the largest gene in the drosophila genome with numerous isoforms that have remained largely unexplored [15]. Cnn has been well studied in a number of cell biology contexts including fly embryos, isolated neuroblasts, as well as the drosophila Schneider 2 cell line. Fluorescence recovery after photo-bleaching experiments in drosophila embryos demonstrate that Cnn exchanges rapidly starting immediately at the center of centrosome and then spreading outward to the edges of the PCM [16]. Phosphorylation in the middle region of Cnn has been shown to play role in the proteins exchange in embryos and there is evidence that this phosphorylation drives higher order assemblies Cnn [16].

Other notable features of Cnn are two conserved motifs – one at the amino terminus of the protein, CM1, and one at the carboxyl terminus of the protein, CM2. CM1 is conserved from the yeast SPB protein, Spc110, all the way to the human homologue CDK5RAP2. CM1 has been found to be important for binding the γtubulin ring complex (γTuRC) and nonsense mutations in Cnn completely disrupt the recruitment of γtubulin and cause abnormal spindles. Though the exact contacts between the γTuRC and CM1 have not been resolved, a high resolution electron microscope structure of Spc110 containing CM1 and the complete γTuRC has been solved [17]. Furthermore, beautiful *in vitro* work has shown that higher order oligomerization of Spc110 is coupled to assembly of the γTuRC [18]. Though the SPB and the centrosome may not

necessarily follow the same mechanisms of assembly, this behavior of Spc110 raises the intriguing possibility that oligomer state of Cnn is also tied to its function of tethering the γTuRC to the centrosome.

Another *in vitro* system that is relevant to Cnn studies is the *C.elegans* protein Spd5. Spd5 does not contain CM1 or any sequence conservation with Cnn, however, it is presumed to be the functional analogue due its necessity in proper centrosome assembly [19]. *C. elegans* also express a version of Spd2, though again the sequence conservation with the drosophila version is slim. Work from Hyman lab has explored the behavior of these two proteins in an *in vitro* setting, to date the only work on purified full length PCM proteins (aside from polo kinases) [20]. These *in vitro* studies reveal that Spd5 alone forms networks of protein as seen by electron micrographs and optical microscopy. Furthermore, addition of Spd2 and polo-like kinase accelerate the formation of this protein network. The observed network of protein is highly reminiscent of the amorphous cloud of protein seen in cryo-tomograms of purified centrosomes. This work suggests that Cnn, itself, is also capable of forming a network that is regulated by Spd2 and polo kinase. However, the nature of the molecular contacts that give raise to these networks is unknown both in the context of Spd5 and Cnn.

Trying to understand the molecular details that give raise to Cnn distributions in the centrosome and in particular, as driven by the CM2 motif is the subject of this thesis and the work presented in the following chapters.

References

1. https://www.biozentrum.uni-wuerzburg.de/zeb/research/topics/theodor-boveri/a-virtual-boveri-library/
2. Guy De-Thi. Cytoplasmic microtubules in different animal cells. The Journal of Cell Biology. 1964, Volume 23, 265-275.
3. Policard A, Bessis M. The centrosome of leukocytes of vertebrates studied by phase contrast microcinematography and by electron microscopy. C R Hebd Seances Acad Sci. 1952 Feb 25;234(9):913-5. PMID:12979250
4. Kollman JM, Polka JK, Zelter A, Davis TN, Agard DA. Microtubule nucleating gamma-TuSC assembles structures with 13-fold microtubule-like symmetry. Nature. 2010.
5. Jaspersen SL, Winey M. The budding yeast spindle pole body: structure, duplication, and function. Annual Review of Cell and Developmental Biology. 2004 20:1-28. PMID: 15473833 DOI:10.1146/annurev.cellbio.20.022003.114106
6. Andersen JS, Wilkinson CJ, Mayor T, Mortensen P, Nigg EA, Mann M. Proteomic characterization of the human centrosome by protein correlation profiling. Nature Publishing Group. 2003 Dec 4; 426 (6966):570–4.
7. Müller H, Schmidt D, Steinbrink S, Mirgorodskaya E, Lehmann V, Habermann K, Dreher F, Gustavsson N, Kessler T, Lehrach H, Herwig R, Gobom J, Ploubidou A, Boutros M, Lange BM. Proteomic and functional analysis of the mitotic Drosophila centrosome. EMBO. 2010 Oct 6; 29(19) 3344-57.

8. Nido GS, Mendez R, Pascual-Garcia A, Abia D, Bastolla U. Protein disorder in the centrosome correlates with complexity in cell types number. Molecular Biosystems, 8 (2012), pp. 353-367.
9. Dobbelaere J, Josue´ F, Suijkerbuijk S, Baum B, Tapon N, Raff J. A Genome-Wide RNAi Screen to Dis- sect Centriole Duplication and Centrosome Maturation in Drosophila. Schliwa M, editor. PLoS Biol. 2008 Sep 16; 6(9):e224. https://doi.org/10.1371/journal.pbio.0060224 PMID: 18798690
10. Gopalakrishnan J; Mennella V; Blachon S; Zhai B; Smith AH; Megraw TL; Nicastro D; Gygi SP; Agard DA; Avidor-Reiss T. Sas-4 provides a scaffold for cytoplasmic complexes and tethers them in a centrosome. *Nature communications*. 2011. 2, 359.
11. Conduit PT, Brunk K, Dobbelaere J, Dix CI, Lucas EP, Raff JW. Centrioles regulate centrosome size by controlling the rate of Cnn incorporation into the PCM. Curr Biol. 2010 Dec 21;20(24):2178-86. doi: 10.1016/j.cub.2010.11.011.
12. Mennella V, Keszthelyi B, McDonald KL, Chhun B, Kan F, Rogers GC, et al. Subdiffraction-resolution fluorescence microscopy reveals a domain of the centrosome critical for pericentriolar material organization. Nature Cell Biology. Nature Publishing Group; 2012 Oct 21; 14(11):1159-68.
13. Fu J, Glover DM. Structured illumination of the interface between centriole and peri-centriolar material. Open Biology. 2012 Aug 1; 2(8):120104–4. https://doi.org/10.1098/rsob.120104 PMID: 22977736

14. Lawo S, Hasegan M, Gupta GD, Pelletier L. Subdiffraction imaging of centrosomes reveals higher- order organizational features of pericentriolar material. Nature Cell Biology. Nature Publishing Group; 2012 Oct 21; 14(11):1148–58.

15. Eisman RC, Phelps MA, Kaufman TC. Centrosomin: a complex mix of long and short isoforms is required for centrosome function during early development in Drosophila melanogaster. Genetics. 2009 Aug;182(4):979-97. doi: 10.1534/genetics.109.103887

16. Conduit PT, Feng Z, Richens JH, Baumbach J, Wainman A, Bakshi SD, Dobbelaere J, Johnson S, Lea SM, Raff JW. The centrosome specific phosphorylation of Cnn by Polo /Plk1 drives Cnn scaffold assembly and centrosome maturation. Dev Cell. 2014 Mar 31;28(6):659-69. doi: 10.1016/j.devcel.2014.02.013.

17. Kollman JM[1], Polka JK, Zelter A, Davis TN, Agard DA. Microtubule nucleating gamma-TuSC assembles structures with 13-fold microtubule-like symmetry. Nature. 2010 Aug 12;466(7308):879-82. doi: 10.1038/nature09207

18. Lyon AS[1], Morin G[2], Moritz M[1], Yabut KC[2], Vojnar T[2], Zelter A[2], Muller E[2], Davis TN[2], Agard DA[3]. Higher-order oligomerization of Spc110p drives γ-tubulin ring complex assembly. Mol Biol Cell. 2016 Jul 15;27(14):2245-58. doi: 10.1091/mbc.E16-02-0072.

19. Hamill DR, Severson AF, Carter JC, Bowerman B. Centrosome maturation and mitotic spindle assembly in C. elegans require SPD-5, a protein with multiple coiled-coil domains. Developmental Cell. 2002 Nov; 3(5):673–84. PMID: 12431374

20. Woodruff JB, Wueseke O, Viscardi V, Mahamid J, Ochoa SD, Bunkenborg J, Widlund PO, Pozniakovsky A, Zanin E, Bahmanyar S, Zinke A, Hong SH, Decker M, Baumeister W, Andersen JS, Oegema K, Hyman AA. Centrosomes. Regulated assembly of a

supramolecular centrosome scaffold in vitro. Science. 2015 May 15;348(6236):808-12. doi: 10.1126/science.aaa3923.

Chapter II- The centrosomin CM2 domain is a multifunctional binding domain with distinct cell cycle roles.

Preface & Contributing Authors

This chapter is composed of the full text manuscript of work published in *PLoS One* in 2018 under the title "CM2 Domain in Centrosomin is a Multi-Functional Binding Domain with Distinct Roles in the Cell Cycle". The authors of this work are Y.R. Citron (UCSF), C.J. Fagerstrom (NIH), B. Keszthelyi (UCSF), B. Huang (UCSF), N.M. Rusan (NIH), M.J.S. Kelly (UCSF), D.A. Agard (UCSF).

Abstract

The centrosome serves as the main microtubule-organizing center in metazoan cells, yet despite its functional importance, little is known mechanistically about the structure and organizational principles that dictate protein organization in the centrosome. In particular, the protein-protein interactions that allow for the massive structural transition between the tightly organized interphase centrosome and the highly expanded matrix-like arrangement of the mitotic centrosome have been largely uncharacterized. Among the proteins that undergo a major transition is the *Drosophila melanogaster* protein centrosomin that contains a conserved carboxyl terminus motif, CM2. Recent crystal structures have shown this motif to be dimeric and capable of forming an intramolecular interaction with a central region of centrosomin. Here we use a combination of in-cell microscopy and *in vitro* oligomer assessment to show that dimerization is not necessary for CM2 recruitment to the centrosome and that CM2 alone undergoes significant cell cycle dependent rearrangement. We use NMR binding assays to confirm this intramolecular interaction and show that residues involved in solution are consistent

with the published crystal structure and identify L1137 as critical for binding. Additionally, we show for the first time an *in vitro* interaction of CM2 with the *Drosophila* pericentrin-like-protein that exploits the same set of residues as the intramolecular interaction. Furthermore, NMR experiments reveal a calcium sensitive interaction between CM2 and calmodulin. Although unexpected because of sequence divergence, this suggests that centrosomin-mediated assemblies, like the mammalian pericentrin, may be calcium regulated. From these results, we suggest an expanded model where during interphase CM2 interacts with pericentrin-like-protein to form a layer of centrosomin around the centriole wall and that at the onset of mitosis this population acts as a nucleation site of intramolecular centrosomin interactions that support the expansion into the metaphase matrix.

Introduction

The centrosome is composed of hundreds of proteins that coordinate with one another to achieve a nucleation hub for microtubules that rearranges and duplicates as a function of the cell cycle. Until quite recently little molecular detail has been available about the protein-protein interactions that regulate and organize this complex coordination. Several key proteins were identified decades ago via genetic interaction studies [1–4], including the *Drosophila melanogaster* proteins centrosomin (CNN), SPD-2, asterless, and pericentrin-like-protein (PLP) all of which are required for proper recruitment of the microtubule nucleation component γ-tubulin. Although once thought to be amorphous, super-resolution light microscopy has shown that the electron dense cloud that surrounds the centriole (peri-centriolar material or PCM), is organized into distinct protein domains [5–7]. One set of proteins including asterless and PLP, form a toroidal shape that remains close to the centriole wall throughout the cell cycle. A second set of proteins, including SPD-2 and CNN, also forms a ring around the interphase centriole but upon

entrance into mitosis this expands outward from the centriole wall to form a much larger centrosome matrix containing the bulk of CNN and γ-tubulin. These distributions suggest the presence of discreet molecular interactions that define the interphase centrosome by tethering proteins, PLP, CNN, etc. at the centriole wall and that these proteins then act as a nucleation point for multivalent higher-order oligomerization of a subset of proteins at the onset of mitosis. However, this idea has not been fully confirmed and little detail is known on a molecular level about the interactions that would support interphase tethering or mitotic oligomerization. Recent work on *Caenorhabditis elegans* proteins (Spd2 and Spd5) has put forward a model of phase separation as an organizing principle for the mitotic centrosome [8]. These contributions, along with yeast-two-hybrid data identifying a vast network of protein-protein interactions [9], begins to highlight the specific and elaborate protein organization within the PCM, although much of the underlying mechanistic detail is still lacking.

Of particular interest in this complex system is CNN as it takes on both a ring-like distribution in interphase as well as a matrix-like role in mitosis. CNN and its human homologue CDK5RAP2 have consistently been identified as important for recruitment of the γ-tubulin ring complex [1, 2,10] and the related self-assembling Spd5 plays an analogous role in *C. elegans* [11]. Previous work has established that proper CNN recruitment is dependent on PLP [5], and co-immunoprecipitation experiments with the human CDK5RAP2 carboxyl terminus and pericentrin are suggestive of a direct interaction [12,13]. More recent work using yeast- two-hybrid experiments has shown there is indeed a direct interaction between CNN's carboxyl terminus and PLP [14] but to date no *in vitro* characterization has yet been performed. Meanwhile, crystallographic studies have revealed atomic details of a CNN intra-molecular interaction [15]. Both these interactions have been attributed to a conserved motif at the car-

boxyl end of CNN, CM2. We sought to further probe CM2's role in the centrosome in the hopes of understanding how it functions in these interactions and to shed light on the overall principles governing protein organization in the centrosome.

CNN contains two highly conserved motifs, the first of which, CM1, is near the amino terminus (Fig 1A) and has been shown to interact with the γ-tubulin ring complex [10, 16] with even conserved yeast motif with the same functionality [17]. The second motif, CM2, is positioned near the carboxyl terminus (Fig 1A). Recent work by Feng *et al*. [15] revealed that *Drosophila* CM2 is dimeric and identified key dimerization residues. Their crystal structures of CM2 show it is predominately helical and forms a complex with the middle portion of CNN (aa490-544) containing a leucine zipper (CNNLZ). Here we confirm the dimerization *in vitro*, further define the requirements for dimerization, and analyze the implications of oligomerization for recruitment to the interphase and mitotic centrosomes in cells. By solution NMR we show that the CM2-CNNLZ complex forms in solution and that *in vitro* CM2 is multifunctional, with the ability to bind a region from the middle of pericentrin-like-protein (PLP) as well as calmodulin (CaM), suggesting that these interactions are mutually exclusive.

Results and discussion

To examine the ability of the c-terminus to form higher order oligomers and determine if CM2 alone can be recruited to the centrosome, two constructs were produced by recombinant expression in *E.coli* and purified. The first was designed to start at beginning of the predicted coiled-coil region in CNN that also coincides with highest sequence conservation (Fig 1A and 1B) and extends to the C-terminus (aa1090-1148). The second construct (aa1064-1148) includes this same region but contains an additional 24 N-terminal residues that are not predicted to be

coiled coil (Fig 1A and 1B). This construct includes the residues identified by Feng *et al*. as being important for dimerization. Size exclusion chromatography with multi-angle light scattering (SEC-MALS) analysis of these two constructs reveals that while the shorter construct is monomeric, the addition of the 24 N-terminal residues results in dimer formation (Fig 1B). Furthermore, a construct with intermediate boundaries (aa1074-1148) remains dimeric (Fig 1C, blue) even at submicromolar concentrations. This construct was used as a dimeric construct for further *in vitro* studies while the longer dimer (aa1064-1148) was used for all further in cell assays. To test if the C-terminus contributes to dimerization, a construct with the final 18 C-terminal residues removed (CM2 Δ1130–1148) was assayed and was also found to be dimeric at submicromolar concentrations (Fig 1C, red). These data, implicating residues 1074–1089 as being essential for dimerization, are consistent with Feng *et al*.'s observations and further suggests that the region of highest sequence conservation (aa1090-1148) is not important for dimerization but rather for interaction with partners.

To determine if both the monomeric and dimeric versions of CM2 are competent to be recruited to the centrosome throughout the cell cycle, GFP fusions of both constructs were made and transiently transfected into *Drosophila* Schneider 2 (S2) cells under the Sas6 promoter as previously described [18]. Cells were co-stained with anti γ-tubulin antibodies and DAPI and assessed for co-localization of GFP with γ-tubulin. In mitotic cells, both the monomeric and dimeric constructs are capable of being recruited to the centrosome with co-localization seen in 95% and 90% of cells, respectively.

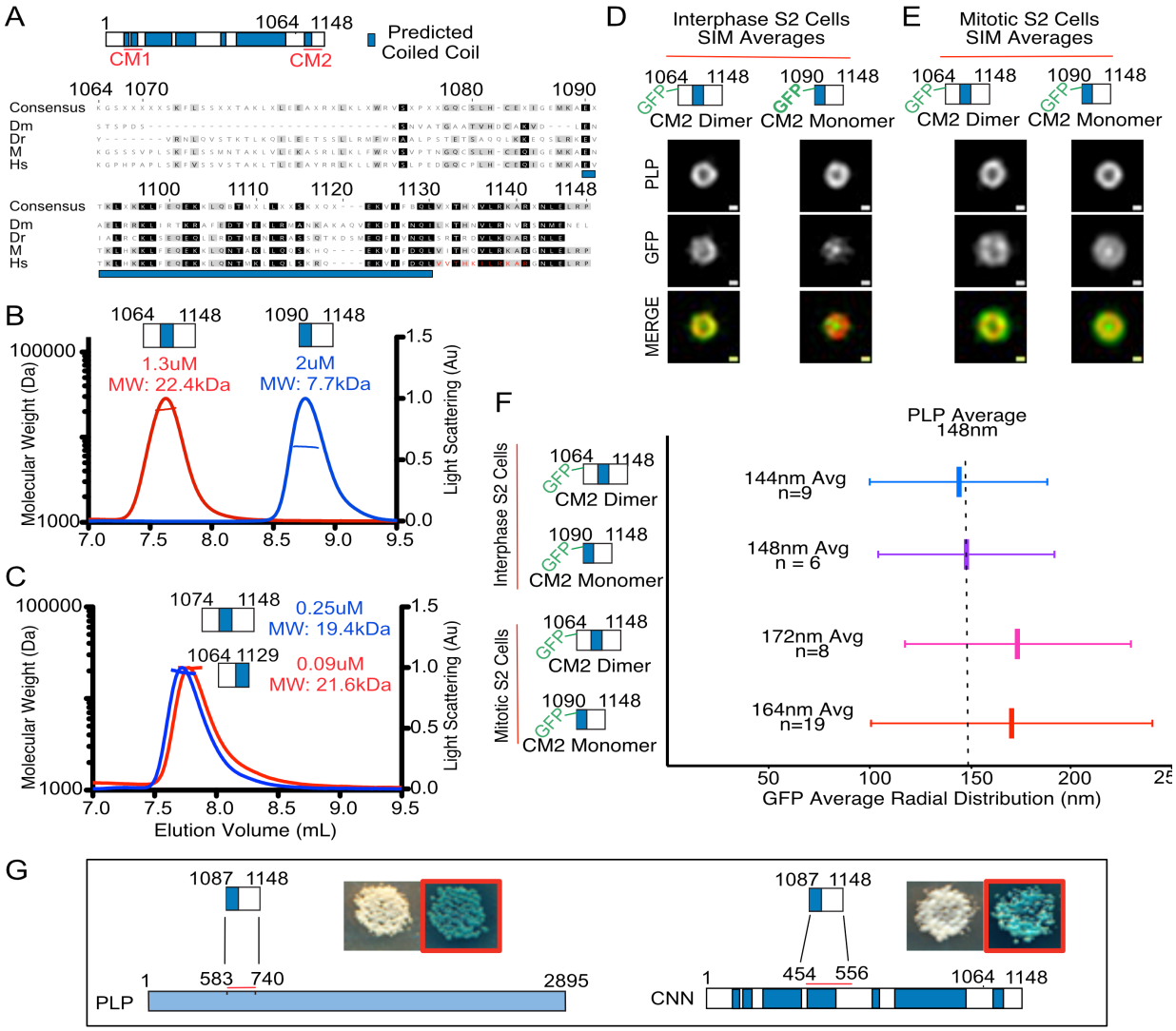

Fig 1. Conserved domain, CM2, of centrosomin characterized by SEC-MALS, SIM, and yeast-two-hybrid experiments. (A) Schematic of Centrosomin with coiled-coil prediction shown in blue. CM1 and CM2 are highlighted in red. Alignment of *D. Melanogaster's* CM2 with the zebra fish, mouse and human (CDK5RAP2) homologues, with residue numbering according to *D. Melanogaster* residues. Higher conservation can be seen starting at residue E1090 in line with the start of the predicted coiled coil region. The predicted calmodulin binding site in human CDK5RAP2 is shown in red. (B) Molecular weights (left axis) measured with SEC-MALS are consistent with aa1064-1148 forming a dimer of CM2 (red) with a predicted monomer weight of 11kDa and a calculated weight of 22.4kDa. The construct aa1090-1148 exists as monomer (blue) with a predicted monomer weight of 7kDa and a calculated weight of 7.7kDa. (C) SEC-MALS of a more minimal dimer construct aa1074-1148 (blue) that has a calculated molecular weight of 19.4kDa and predicted monomer weight of 9kDa. A construct with the final 18 residues truncated (Δ1130–1148) maintains a dimeric oligomer state (red) with a calculated molecular weight of 21.6kDa and predicted monomer weight of 8.8kDA. (D) Z-projections of the aligned and averaged PLP and GFP distributions for both the monomer and dimer GFP-CM2 fusion constructs in interphase S2 cells. Scale bar represents 100nm. (E) Z-projections of the monomer

and dimer GFP-CM2 fusion constructs in mitotic S2 cells. Scale bar represents 100nm (F) Radial averages of the data represented in figures D and E with vertical bars indicating the average and horizontal bars representing the standard deviation of the Gaussian fit. (G) Schematic summaries of yeast-two-hybrid experiments showing the CM2 construct (aa1087-1148) interacting with a minimal domain of PLP (aa583-740) and the middle domain of CNN (aa454-556). Yeast plates of the interaction test are shown with red boxes indicating plating on selection media.

Structured Illumination Microscopy (SIM) was used to assess GFP distributions in higher resolution at both interphase and mitosis. SIM images were aligned, averaged and fit with a Gaussian to obtain a radial average using previously described methods [5]. At interphase both the monomeric and dimeric constructs have tight toroidal distributions similar to that of PLP (Fig 1D and 1F), peaking at around 148nm, as would be expected for an interphase interaction between CM2 and PLP. On the other hand, during mitosis the monomeric and dimeric CM2 versions have both a larger radial average (164nm and 172nm, respectively) and a broader distribution (Fig 1E and 1F) similar to full length CNN. These data suggests that CM2 alone is sufficient to integrate into the mitotic centrosome and given the presence of endogenous CNN is consistent with an intramolecular interaction between CM2 and the middle region of CNN. Though it had been known that full-length CNN underwent this change in distribution, our data newly indicate that CM2 itself is important for CNN's recruitment both at interphase and at mitosis. We note that the averaged monomeric CM2 distributions at mitosis and interphase show a bright intensity at the center of the centrosome that does not appear in the dimer aver- ages. While the origins of this central peak are unknown, the overall behavior indicates that a dimer interface is not necessary for recruitment although it may serve to increase the effective affinity. The striking difference in organization at these two cell cycle stages is suggestive of distinct molecular mechanisms, raising the possibility that two distinct binding partners maybe utilized to mediate recruitment at different times in the cell cycle.

Previous yeast-two-hybrid studies have been instrumental in identifying interaction partners critical for centrosome organization and for narrowing down the regions of interaction. These studies have shown that CM2 interacts with PLP aa583-1376 and that this interaction is not required for PLP recruitment to the centrosome but is essential for localizing PLP to centrosome flares within the PCM matrix [14]. To narrow down the region of PLP interacting with CM2 and confirm that it is the CM2 region that is was responsible for both intra- and intermolecular CNN interaction, a refined yeast-two-hybrid screen was carried out (S1 Fig shows details). These experiments revealed that monomeric CNN was indeed capable of binding CM2 interaction partners and identified a minimal interaction region between monomeric CM2 and the central portion of CNN (residues 454–556, Fig 1G). This is in agreement with Feng *et al*.'s observations of interaction between the same central fragment (termed CNNLZ) and dimeric CM2. Additionally, the yeast two-hybrid analysis narrowed down the PLP-CM2 interaction region to a short stretch of PLP (PLPMD, aa583-740, Fig 1G). For a full list of constructs used in the yeast-two-hybrid experiments see S1 Fig.

To examine these interactions at higher resolution *in vitro*, the middle regions of CNN and PLP were fused to the GB1 solubility tag, purified and tested for CM2 interaction by observing changes in CM2 resonances in 2D [^{15}N, ^{1}H] NMR HSQC spectra. As a first step, the backbone resonances of monomeric CM2 (aa1090-1148) were assigned (BMRB: 27206) using standard triple resonance and residue-specific NMR experiments. Overlaying the HSQC spectra from monomeric and dimeric CM2 (aa1074-1148) reveals that the resonances of the final 40 C-ter- minal residues are unchanged between the monomer and dimer states (Fig 2A and 2B), allowing the assignment of a significant number of residues in the dimer. From this result we infer that the structure of the C-terminal region of CM2 is unchanged upon dimerization,

otherwise significant changes in chemical shift would have been observed. The region that does change in our spectra is quite consistent with the dimerization seen in the crystal structure (PDB 5MWE) of a complex between dimeric CM2 and a middle domain of CNN (Feng *et al*). Unfortunately, further interpretation of the dimer was hampered by significant variability in the dimer spectra that we attribute to multiple dimer species and/or multiple conformations. In support of this, both we (S2 Fig) and Feng *et al*. observed multiple dimer species by SEC-MALS at micromolar CM2 concentrations. Given that the monomer was sufficient in the two-hybrid studies, we used the monomer to explore solution interactions with binding partners.

To assess the ability of monomeric CM2 to bind CNNLZ in solution we used the same CNNLZ fragment reported in the Feng *et al*. crystal structure (aa490-567, PDB:5MWE), while for the PLPMD we used the fragment defined by the yeast two-hybrid screen (aa583-740, Fig 1E). 2D ^{15}N HSQC spectra of monomeric ^{15}N labeled CM2 (aa1090-1148) were collected in the absence or presence of 150μM CNNLZ (purple) or 200μM PLPMD (pink) (Fig 2C). Addition of the GB1solubility tag alone showed negligible changes in the 2D ^{15}N –HSQC spectra of CM2 (S3 Fig). In the presence of CNNLZ, multiple cross peaks are shifted and are concentrated into three patches when mapped onto the structure of CM2 in complex with CNNLZ (PDB 5MWE) (Fig 2D and 2F). The first patch of residues (aa1092-1110) showing strong chemical shift perturbations is the very same region that changed upon dimerization. As previously noted, this also corresponds to the dimer contact observed in the crystal structure. Thus, binding to CNNLZ is sufficient to stabilize dimer formation even in the truncated CM2.

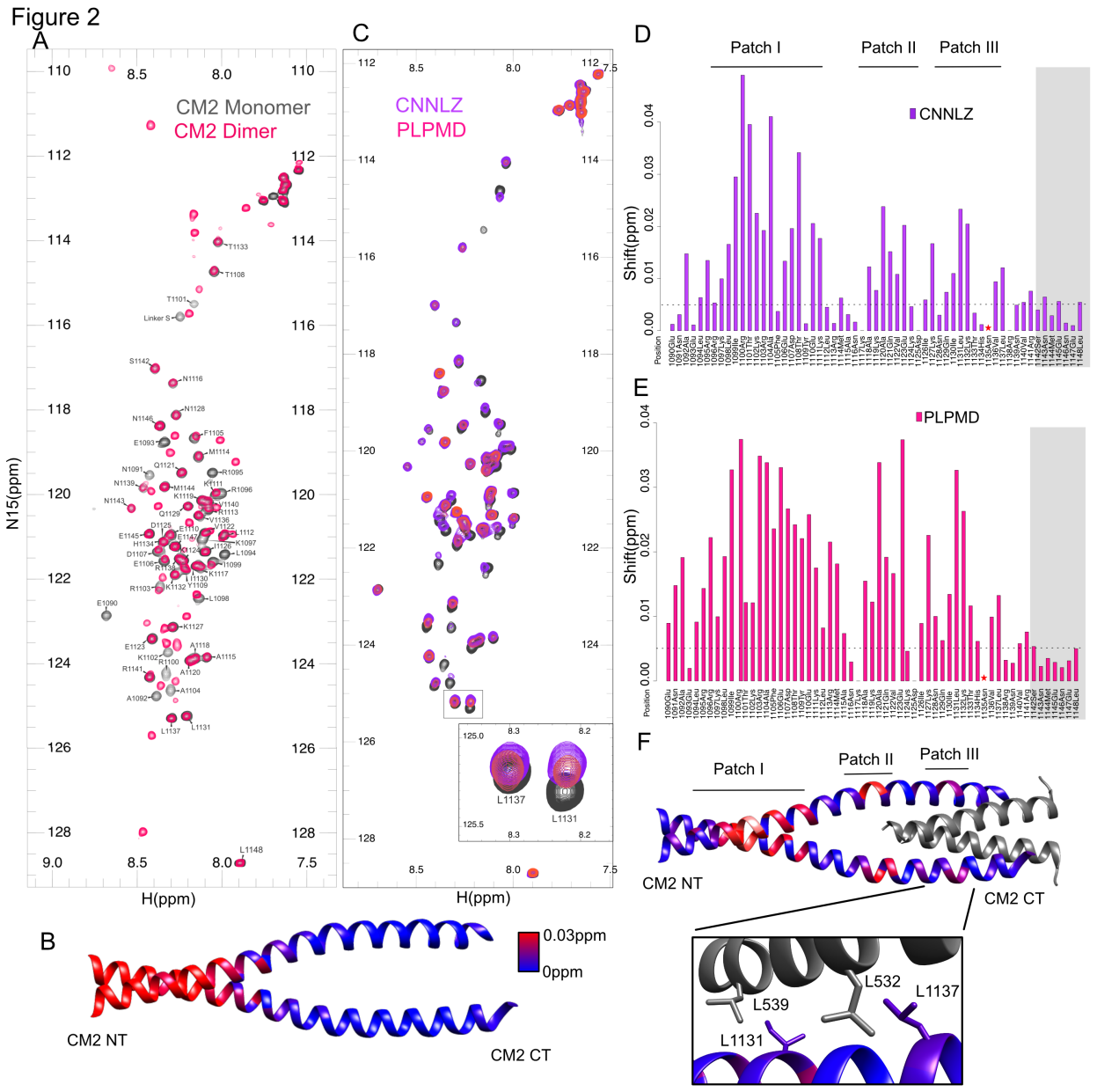

Fig 2. 2D ^{15}N-HSQC spectra of assigned monomeric CM2 shows interaction along three patches of residues. (A) Overlays of 2D ^{15}N-HSQC spectra and assignments of CM2 monomer (gray) and dimer (pink) showing the peaks corresponding to residues F1105-L1148 have identical chemical shifts. All backbone monomer peaks are assigned. Though N1135 does appear in backbone tracing experiments, it does not appear in HSQC spectra. (B) Mapping of the combined chemical shift differences (blue to red) between the monomer and dimer HSQC spectra onto the crystal structure of CM2 (pdb:5MWE). Peaks that were not present in the dimer HSQC spectra were arbitrarily colored as a combined chemical shift difference of 0.1ppm for

visualization purposes. (C) Overlay of monomer CM2 (gray) with 200μM PLPMD (pink) and 150μM of CNNLZ (purple) illustrates chemical shift changes, particularly for L1131 and L1137 (inset). (D) Quantitation of the combined chemical shift changes of CNNLZ (purple) compared to monomeric CM2 alone reveals three regions with greatest shift changes. Dashed line indicates a combined chemical shift change of 0.0025ppm. The star indicates residue N1135 that is not visible in the HSQC spectra. Gray shading indicates the residues that are not modeled in the crystal structure (pdb:5MWE). (E) Quantitation of chemical shift changes of PLPMD (pink) compared to monomeric CM2. (F) Combined chemical shift changes of CM2 in the presence of CNNLZ mapped onto the crystal structure of CM2 with CNNLZ (pdb:5MWE). CM2 is colored blue to red in proportion to chemical shift changes. CNNLZ is shown in gray. Inset shows the interface between CM2 and CNNLZ and the proximity of I1130 to L539 and L1137 to L532.

The third patch is close to the C-terminus and includes several well-conserved hydrophobic residues (I1130/L1131/V1136/L1137). As shown by the crystal structure (Fig 2F) these residues are in a region buried in the interface between CM2 and CNNLZ. In particular, we see shifts for the backbone $^{1}H_{N}$, ^{15}N resonances of I1130/L1131 and L1137, which are located in close proximity to CNNLZ's L532 and L539 residues in the crystal structure (Fig 2D, inset). The importance of these residues is also consistent with Feng *et al*.'s mutation analysis in cells showing that L532E and L539E mutants disrupt CM2's recruitment to the pericentriolar material. Notably, the second patch is adjacent to the end of CNNLZ's structured region leading us to hypothesize that though not seen in the crystal structure, some portion of the remaining 23 residues of CNNLZ must be interacting with the CM2 patch II region.

Interestingly, addition of PLPMD results in significant peak shifts for a remarkably similar set of CM2 residues. These residues map onto the same three patches (Fig 2E), again indicating that PLPMD stabilizes CM2 dimerization. Although there is no structural information for PLPMD, it is predicted to contain a coiled-coil stretch (S4 Fig) according to the COILS prediction server (http://www.ch.embnet.org/software/COILS_form.html). Thus like CNNLZ,

PLPMD is presumably dimeric and contains a helical region that binds analogously to the same residues in CM2 as does CNNLZ. Similar experiments using dimeric CM2 in the presence of PLPMD and CNNLZ show significant reductions in peak intensities (S5 Fig), however, localizing those changes to particular residues is difficult for the reasons mentioned above. Together, these experiments indicate that two helical regions of CM2 not involved in dimerization form a binding surface for both intramolecular interactions (CNNLZ) and intermolecular interactions (PLPMD).

Because the human homologue of CNN, CDK5RAP2, contains a predicted CaM binding site in its CM2 domain and immunoprecipitation experiments have confirmed this interaction [13], we asked if *Drosophila* CM2 might also bind CaM using the same NMR assay, despite the lack of a canonical CaM binding motif. In the presence of 20μM CaM and 2mM $CaCl_2$ the CM2 HSQC spectra shows significant perturbation (Fig 3A, pink). These shifts depend on CaM concentration, and even at concentrations as low as 5μM, peak shifts can be measured (Fig 3B) suggesting that the affinity of CaM for CM2 is quite high and significantly greater than either *E. coli* produced CNNLZ or PLPMD. Mapping the chemical shifts onto the 5MWE crystal structure reveals shifts concentrated in the same patches as in the presence of CNNLZ and PLPMD, as well as additional shifts along the length of the helices. As the shifted regions are also consistent with dimer interactions, we speculate that CaM is even more potent at dimerizing monomeric CM2 than either CNNLZ or PLPMD. Our NMR chemical shift perturbations indicate CaM binds the hydrophobic residues at the CM2 C-terminus. This is also consistent with the known requirement for hydrophobic residues in calcium dependent CaM binding though the patterning of hydrophobic residues in CM2 is not ideal [19]. To assess the effect of calcium on binding, experiments were performed with 2mM EGTA added in place of 2mM $CaCl_2$ (Fig 3A, purple).

Under these conditions the chemical shift perturbations are significantly reduced but are not completely absent. Based on comparison of chemical shifts under EGTA conditions and titrations of CaM in the presence of calcium, we estimate that the apparent affinity in the absence of calcium is reduced by 50–70%. HSQC spectra of CM2 in absence of calmodulin but with 2mM EGTA do not show significant chemical shift perturbations compared to spectra in the presence of calcium, indicating that calcium by itself does not have an effect on CM2 structure (S6 Fig). As with PLPMD and CNNLZ binding, ^{15}N labeled dimeric CM2 shows very significant reductions in peak intensity upon CaM addition for a number of residues (S7 Fig), which are likely due to cross peak broadening. Though these experiments support a calcium dependent CaM interaction, gaining a better understanding of the mechanism and function of this interaction will require further structural and cellular studies.

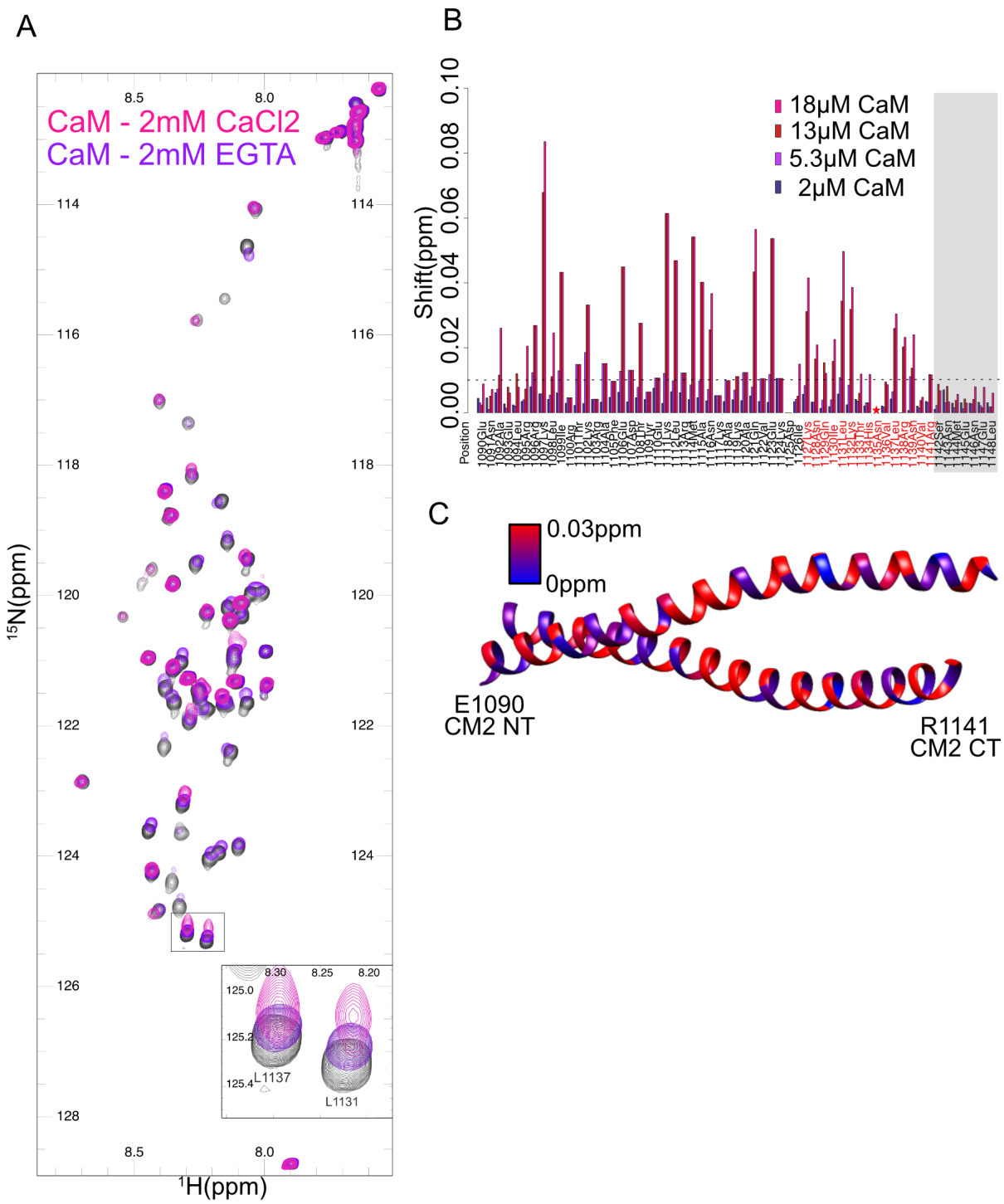

Fig 3. 2D ^{15}N-HSQC spectra of monomeric CM2 show a calcium sensitive interaction of calmodulin. (A) 2D ^{15}N-HSQC spectra of monomeric CM2 alone (gray) overlaid with the spectra after the addition of 18μM CaM with 2mM CaCl2 (pink) shows significant shifts. While 18μM CaM in the presence of 2mM EGTA (purple) shows more minimal shifts. Inset: Shifts on

leucine 1131 and leucine 1137 are apparent. (B) Quantitation of shifts from a CaM titration (2mM $CaCl_2$) where several shifts are greater than 0.01ppm (dashed line) on addition of 5.3μM CaM. Residues that align with the predicted CaM binding site in mammalian CDK5RAP2 are shown in red. The star indicated residue N1135 that is not visible in the HSQC spectra while the gray shading indicates residues that are not modeled in the 5MWE crystal structure. (C) Mapping of chemical shift changes (blue-red) onto the 5MWE crystal structure (CNNLZ is shown in gray) reveals shifts along the length of the helices including the region where dimer contacts are made.

To interrogate in greater detail the functional contributions of specific regions and residues implicated by the HSQC binding data, truncations and mutations were designed in GFP fusions of dimeric CM2 and assessed in S2 cells. Firstly, to determine if the most carboxyl terminal residues were required for recruitment, a truncation at residue 1130 was made in the GFP-dimeric CM2 construct (Fig 4A, CM2 Δ1130–1148) and localization to the centrosome was completely abolished (Fig 4B). Maximum GFP pixel intensities in regions identified as the centrosome by γ-tubulin staining show an 85% reduction in maximum intensities when compared to the wildtype CM2 construct (Fig 4B). By contrast, removal of the final 7 residues (CM2 Δ1142–1148) had no effect on centrosome recruitment, despite their high level of conservation. This is consistent with our HSQC experiments showing minimal changes in this region upon CNNLZ binding (Figs 2C, 2E and 3B). To investigate the role of the intermediate residues, alanine scanning was performed in blocks of four residues across the relevant region (aa1130-1141). While mutating the span RNVR (Fig 4A) to alanines did not reduce the ability of CM2 to localize at the centrosome, mutating either the ILKT block or the HNVL block significantly reduced recruitment by 29% and 55%, respectively (Fig 4B). These data are in agreement with our HSQC data that show significant shifts in leucines 1131 and 1137 that are contained within these spans. Furthermore, a single point mutant replacing leucine 1137 with an alanine nearly abolished recruitment, reducing the maximum pixel intensity by 80% (Fig 4B and 4C).

Importantly, a more conservative mutation of L1137 to a valine shows a partial recovery of recruitment, suggesting a critical hydrophobic interaction is mediated by this residue (Fig 4B).

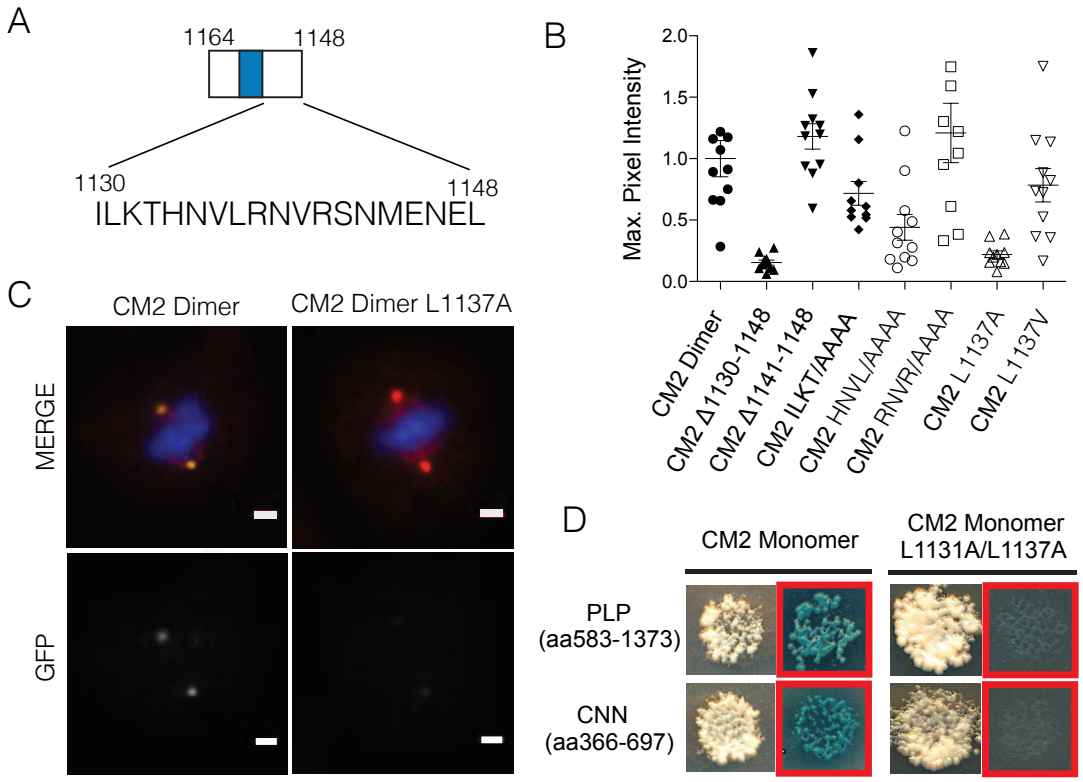

Fig 4. Leucines 1131 and 1137 implicated as important for CM2 interaction with CNNLZ and PLP. (A) Schematic of dimeric CM2 with residues 1130-1148 highlighted. (B) Quantification of the maximum GFP pixel intensity at the centrosome normalized to dimeric CM2 (aa1064-1148). From the left, GFP-CM2 dimer fusion serves as the control to which all other GFP constructs are compared. Truncating off the final 18 residues, CM2 Δ1130-1148, shows an abolishment of recruitment to the centrosome while truncating the final 7 residues, CM2 Δ1141-1148, has no apparent effect on recruitment. An alanine mutant constructs of ILKT to AAAA and HNVL to AAAA have 28% and 56% reduction in GFP intensity respectively, while RNVR to AAAA appears unperturbed. Single point mutations of L1137 to alanine and valine have 78% and 27% reductions, respectively. (C) Representative wide field microscopy images of wildtype CM2 dimer (left) with identical scaling and contrast of CM2 dimer L1137A point (right) mutation images. The top row shows merging of DAPI (blue), γtubulin (red) and GFP (green) while the bottom is only the GFP channel. 1um scale bar. (D) Yeast-two-hybrid plates comparing monomeric CM2 prey – PLPMD bait colonies and monomeric CM2 prey – CNNMD bait colonies (right) with identical experiments using CM2 double mutant L1131A/L1137A (left). Red boxes indicate plating on selection media.

Consistent with these observations, yeast-two-hybrid data with a double L1131A/L1137A mutant show abolishment of the interaction with CNNLZ, but also extended our studies by showing a loss of interaction with PLPMD (Fig 4D). Notably, the yeast-two-hybrid experiments were done with fragments of CNN middle domain and PLPMD significantly larger than the determined minimal domains (Fig 1F) indicating that secondary regions are not contributing to the interaction by contacting CM2 outside patch I. Though Feng *et al*. argue that I1126 and T1133 are also required for interaction with CNNLZ, we see only a minimal perturbation of CM2 recruitment when ILKT is replaced with alanines. This suggests that Feng et al.'s mutation to glutamic acid is strongly disruptive of the hydrophobic pocket required for interaction but that these residues are not actively involved in contacting CNNLZ. Rather, we show that mutation of leucine 1137 alone can abolish recruitment in cells, an observation that is fully consistent with our NMR data showing chemical shift changes for this residue when CM2 binds all three of its interaction partners.

Taken together, our yeast-two-hybrid, cellular microscopy, SEC-MALS experiments and NMR data support a model where CM2 plays distinct roles in interphase and mitosis through interactions with several binding partners and that these are ultimately responsible for the different phases of PCM establishment and expansion. We suggest that during interphase CNN is tethered near the centriole wall via the interaction of CM2 with PLPMD and that upon transition into mitosis the CNNLZ domain of this tethered protein serves as a nucleation point for the formation of a multivalent higher-order assemblies mediated primarily by CM2- CNNLZ interactions, likely in a phosphorylation-dependent manner. Our data suggest that both these interactions exploit the same binding mode with CM2 in order to interact through the con- served residue L1137. The idea that CNNLZ and PLPMD interactions with CM2 are mutually exclusive

is consistent with numerous reports of PLP, not just at the centriole wall, but also at the periphery of the centrosome during mitosis [14, 20]. This distribution of PLP suggests that though PLP is present, it can't incorporate throughout the PCM and that aside from interphase toroidal region it can only bind on the edges where intramolecular CM2 interactions are less likely to take place. Though monomeric CM2 is sufficient to bind both CNNLZ and PLPMD, given the importance of this single residue for both interactions, it is likely that dimeric CM2 is favored in cells by providing increased affinity and refining localization. Furthermore, these data suggest that PLPMD is likely to be a helical dimer that presents itself to CM2 similarly to CNNLZ.

Though we show convincingly that CM2 is also capable of interacting with CaM in a calcium dependent manner, uncovering the functional role of this interaction will require further investigation. Nevertheless, given the high affinity of CaM for CM2 and that HSQC spectra implicate the same hydrophobic residues for all three interactions tested here, CaM may function as a regulatory mechanism that modulates PCM assembly by competing with PLPMD or CNNLZ for binding to CM2.

Materials and methods

Protein expression and purification

CNN cDNA (LD19135) was obtained from the DGRC and sub-cloned into the 6xHIS containing pET28a expression vector modified to replace the TEV cleavage site with a PreCission protease cleavage site. GB1-CnnMD, GB1-PlpMD and GB1 alone were cloned into the same expression vector. For unlabeled protein, *E-coli* was grown in terrific broth at 37℃ to OD_{600}— 0.6–0.8 then induced with 1mM IPTG, cooled to 18℃ and grown for 16-18hours before harvesting.

Samples labeled with ^{15}N or ^{13}C were grown in 3g/L KH_2PO_4, 6g/L Na_2HPO_4, 0.5g/L NaCl, 0.011g/L $CaCl_2$, 0.18g/L $MgSO_4$, 0.001g/L thiamine, 0.001g/L biotin with the addition

of either unenriched or labeled ammonium salt and/or glucose as a carbon source at 1.25g/L (^{15}NH)SO and 2g/L ^{13}C glucose. Cells in labeling media were grown to OD_{600}—0.5 then induced with 1mM IPTG, cooled to 18℃ and grown for 16-18hours before harvesting.

For all proteins, cells were harvested by centrifugation then pellets were either frozen for later use or lysed immediately with a Emulsiflex C3 in 50mM HEPES pH 7.0, 300mM NaCl, 10mM imidazol, and 6mM beta-mercaptoethanol. Lysates were clarified by ultracentrifugation at 35,000xg and the supernatant was incubated with Qiagen NiNTA Superflow resin with gentle agitation for 1.5–2 hours. The resin was washed in batch using 50ml lysis buffer and eluted with a 300mM imidazol buffer. The 6xHIS tagged was cleaved off of CM2 constructs and GB1 alone by overnight incubation with 3C protease (except in the case of CM2 Δ1130–1148). The pooled elution was then further purified by cation exchange chromatography. Additionally, non-labeled proteins were further purified by on size exclusion columns. GB1-CnnLZ and GB1-PlpMD were left with the 6xHIS tag uncleaved and loaded immediately from NiNTA Superflow resin elution onto size exclusion columns.

SEC-MALS

Multi-angle light scattering analysis was performed with a KW-802.5 size exclusion column on an Ettan liquid chromatography system (GE Healthcare Life Sciences) with inline DAWN HELEOS MALS and Optilab rEX differential refractive index detector (Wyatt Technology). All

samples were in 50mM HEPES pH 7.0, 200mM NaCl, and 1mM DTT running buffer. Data were analyzed using ASTRA VI system software (Wyatt Technology).

S2 cell microscopy sample preparation

Relevant genes were cloned into a pMT V5 plasmid (Thermo Fisher) modified to contain the Sas6 promoter directly upstream up the open reading frame as previously described [21]. *Drosophila* Shnieder 2 (S2 cells) from ATCC were transfected using Amaxa Cell Line Nucleofector Kit V (Lonza). After 34–38 hours dimer-CM2 and dimer-CM2-L52A underwent fluorescence flow cytometry and showed equivalent GFP expression but were sorted nonetheless and plated. All other cells were plated after 36 hours on convanavalin-A (sigma) coated glass bottom dishes. Samples for SIM were plated on 35mm glass bottom Delta T dishes (Bioptechs). After 3 hours cells were washed with PBS and fixed in cold methanol for 20min. Cells were then rehydrated in PBS and blocked in PBS with 0.02% tween and 3% BSA. Samples for wide field microscopy were stained 1:500 with rabbit anti-GFP antibodies (Invitrogen) and 1:75 mouse anti γ-tubulin (Sigma GTU88). SIM samples were stained with 1:500 chicken anti-GFP anti- bodies (Invitrogen) and 1:100 anti-PLP (86-PPH-A against aa683-974, a kind gift from Jordan Raff). Fluorescent secondary antibodies Alexa 488 or Alexa 555 were then applied to the sample at 1:500 as well as 300nM DAPI. All samples were mounted in an v/v 90% glycerol, v/v 10% Tris pH 8.0 and w/v 0.5% propyl-gallate media.

Yeast-two-hybrid analysis

Cnn 366–697, Cnn 454–556, Cnn 1087–1148, PLP 583–1373 and PLP 583–740 pieces were amplified from cDNA clones by PCR using Phusion (Thermo Fisher Scientific, Waltham, MA) and with the primers

Cnn 366_F CACCATGTCCTCCAGCGGCCGTTCCATGAGTGAC, Cnn 697_R AGGCGCTGCCAAACTGTTGGAGGTTTC, Cnn 454_F CACCATGGAAGCAGATCTGCAGCAATCCTTCACGGAG, Cnn 556_R TCGATCAGCGGCCAACACGCC,

Cnn 1087_F CACCATGGTAGATCTTGAAAACGCC, Cnn 1148_R TAACTCATTCTCCATGTTTGAGCGAAC,

PLP 583_F for PLP 583–1373 CACCATGTCCCTCTCCTTGGATGAGTC,

PLP 1373_R TGGAGGTAGGGAGGAATGTGTTTTTCCC,

F- BamHI NdeI 583 for PLP 583–740 CACCATGGGATCCCATATGATGCCTTCCCTCTCCTTG GATGAG

PLP 740_R GCGAGTCCTGCGGCCGCTTAACTCGAGCGTTTCACTGCATCG.

PCR products were then introduced into Gateway Entry vectors using the pENTr/D-TOPO Kit (Thermo Fisher Scientific). All Y2H experiments were then conducted as described previously in Galletta et al 2016 [9]. In brief, fragments of Cnn and PLP were introduced into pDEST-pGADT7 and pDEST-pGBKT7 using Gateway technology (Thermo Fisher Scientific), transformed into Y187 or Y2HGold yeast strains (Takara Bio USA, Mountain View, CA), and grown in −*leu* or −*trp* media to select for plasmids. After mating of the two strains, yeast were grown on −*leu*, −*trp* (DDO) plates, then replica plated onto plates of increasing stringency: DDO; −*ade*, −*leu*, −*trp*, −*ura* (QDO); −*leu*, −*trp* plates supplemented with Aureobasidin A (Takara Bio USA) and X-α-Gal (Gold Biotechnology, St. Louis, MO) (DDOXA); and −*ade*, −*leu*, −*trp*, −*ura* plates supplemented with Aureobasidin A and X-α-Gal (QDOXA). Interactions

were scored based on growth and the development of blue color as appropriate. All plasmids were tested for the ability to drive reporter activity in the presence of an empty vector (autoactivation). Plasmids that conferred autoactivity were omitted from further analysis.

Microscopy acquisition and analysis

SIM data was acquired on a DeltaVision OMX SR microscope (GE Healthcare) using a 60x/ 1.42 NA oil immersion PSF objective and three sCMOS cameras. Immersion oil with a refractive index of 1.514 was used to match with the refractive index of the sample. Z stacks of 9μm thickness were collected with 0.125μm step-sizes using 5 phases and 3 angles per image. Reconstructions were preformed using SoftWorx 6.5.2 (GE Healthcare) with a 0.003 Wiener filter for the Alexa Fluor 488 channel and 0.002 Wiener filter for Alexa Fluor 555 as suggested by analysis using the ImageJ plugin SIMcheck [22]. Channel specific optical transfer functions were used for reconstructions. Alignment, averaging and calculation of the radial distribution were performed using custom python scripts previously described [5]. Monomeric CM2 data was fit with an additional central Guassian to distinguish the central intensity from the ring distribution.

Widefield microscopy was acquired on a Ziess Axiovert 200 and GFP intensity was quantified using Matlab. Experiments that were not done in single batch were normalized using GFP quantification of GFP-Dimer CM2.

Nuclear magnetic resonance

Double labeled ($^{13}C/^{15}N$) protein was expressed as described above with ^{15}N ammonium chloride and $^{13}C_6$ glucose and purified. The following 3D triple resonance experiments for

back- bone assignments were recorded on a 500MHz Bruker AVANCE DRX500 spectrometer equipped with a Z-gradient QCI inverse cryoprobe ($^{15}N/^{13}C/^{31}P,^{1}H$): CBCANH (pulse program: cbcanhgpwg3d), CBCAcoNH(pulse program: cbacaconhgpwg3d), and hNcaNHn (pulse program: hncannhgp3d). NMRPipe was used to process 3D spectra [23]. Proton chemical shifts were referenced to an external DSS standard and ^{15}N and ^{13}C shifts referenced indirectly from this value. Double labeled protein was also used to perform the following multiplicity selective in-phase coherence transfer (MUSIC) experiments on a 800 MHz Bruker AVANCEI spectrometer equipped with a Z-gradient TXI cryoprobe: music_qn_3d, music_de_3d, music_ile_3d, music_cm_3d, music_tavi_3d, music_kr_3d[24]. All experiments were performed at 300K in 10mM Trizma pH 7.2, 150mM NaCl, 0.01%(w/v) NaN_3 and 5% (v/v) D_2O.

All 2D [^{15}N, ^{1}H]-HSQC (pulse program: fhsqcf3gpph) binding experiments were carried out with 100μM of ^{15}N labeled protein on an 800 MHz Bruker AVANCEI spectrometer. HSQC experiments were performed at 300K with all proteins dialyzed overnight into 20mM PIPES pH 6.8, 140mM NaCl, 0.01% (w/v) NaN_3, 5% (v/v) D_2O and unless otherwise noted contained 2mM $CaCl_2$.

Resonance assignments and analysis was done in CCPNMR [25]. Peak intensities and shifts were analyzed and plotted in R. Combined chemical shift were calculated using the formula $\Delta\delta(^{1}H) + \Delta\delta(^{15}N)/5$ as described by Hajduk et *al*. [26].

Supporting information

Supplemental Figure 1- Schematic of All Yeast-Two-Hybrid Experiments

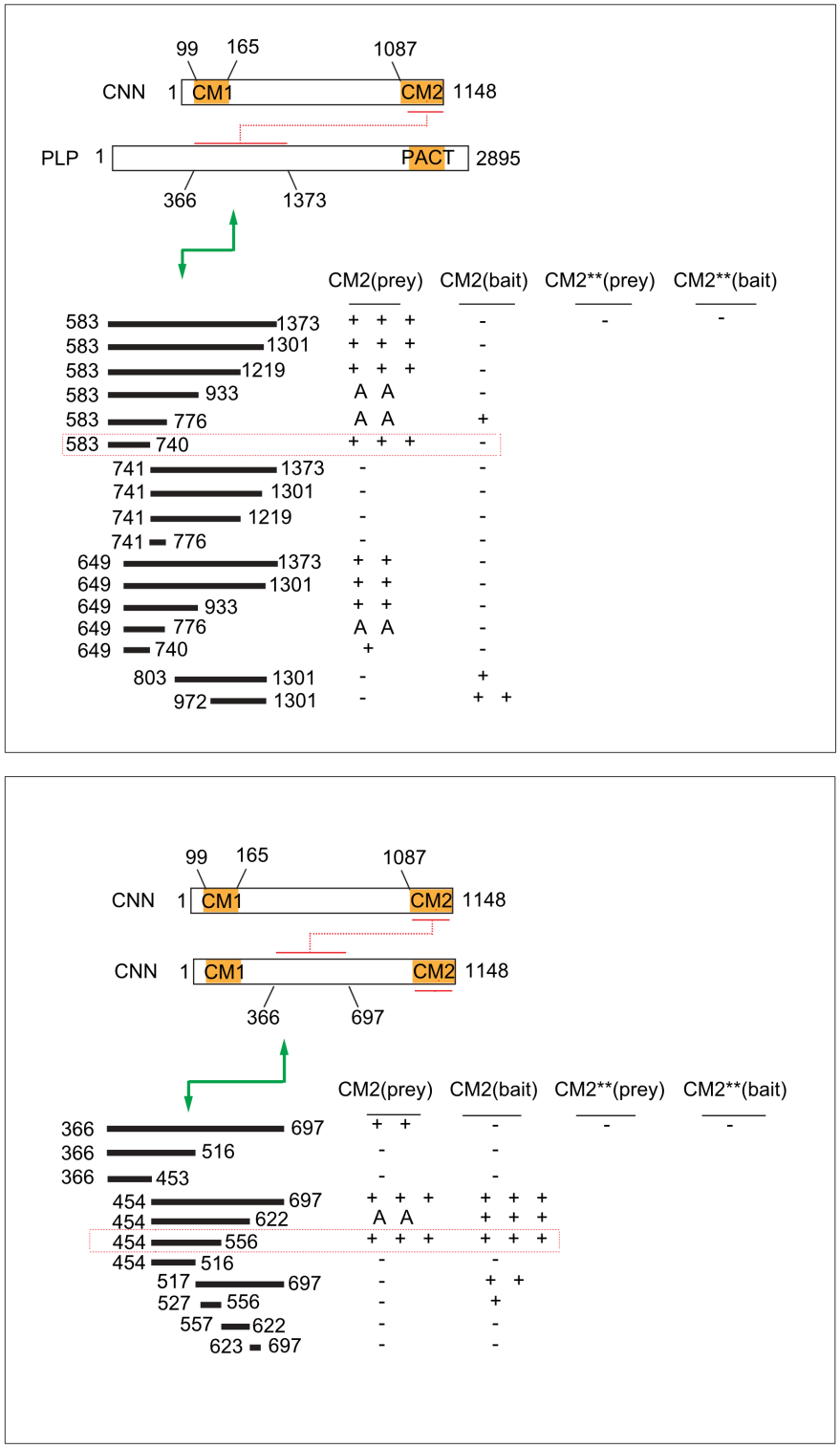

S1 Fig. Schematic of all yeast-two-hybrid experiments.

Supplemental Figure 2 - SEC-MALS of CM2 (aa1074-1148) Indicates Multiple Dimer Species

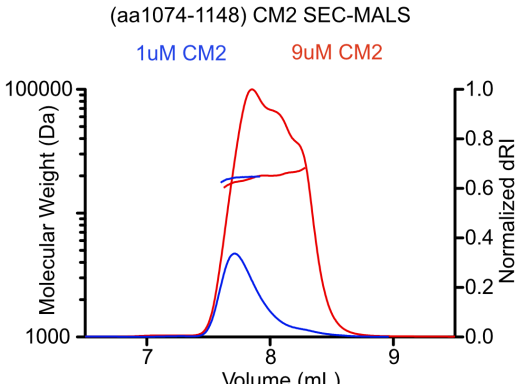

S2 Fig. SEC-MALS of CM2 aa1074-1148 indicates multiple dimer species. CM2 construct used for NMR appears dimeric by SEC-MALS analysis. At 1µM (blue) this construct appears a predominately, as a single dimeric peak with a calculated molecular weight of 19.2kDa while the predicted monomer weight is 9kDa. At 9µM (red) this same construct appears as three or more not fully resolved peaks, however, the molecular weight across all these peaks appears to remain dimeric.

Supplemental Figure 3 - GB1 Control 2D ^{15}N-HSQC Experiment

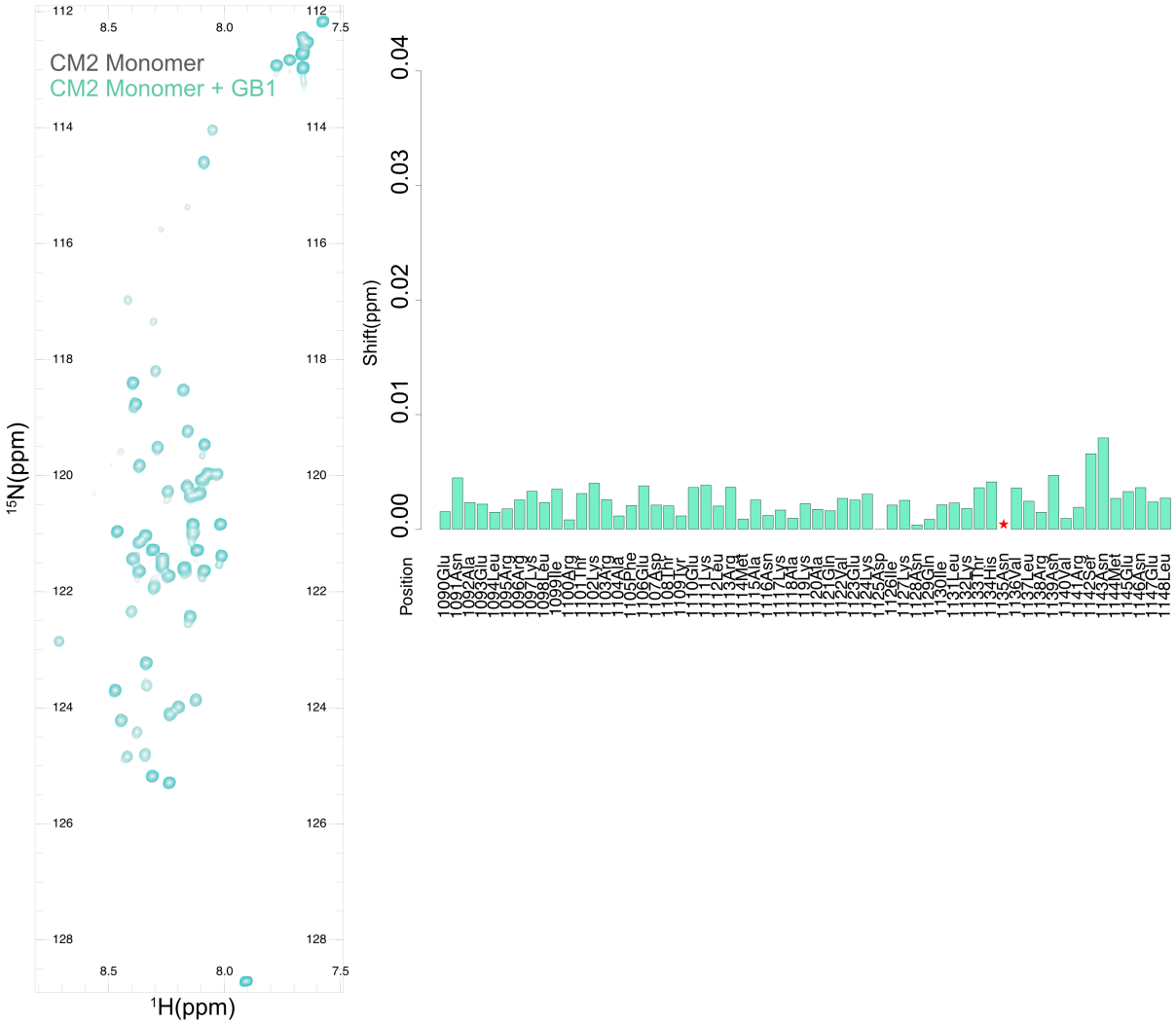

S3 Fig. GB1 control 2D ^{15}N-HSQC experiment. (A) HSQC spectra from a control experiment of monomeric CM2 (gray) and monomeric CM2 with 150μM GB1 (cyan) overlaid. All the peaks appear unperturbed in the presence of GB1. B) Quantitation of peak shifts on addition of GB1 with the same y-axis scaling as for the GB1-CNNLZ and GB1-PLPMD data in Fig 2D and 2E.

Supplemental Figure 4 - Coiled-Coil Prediction of PLPMD

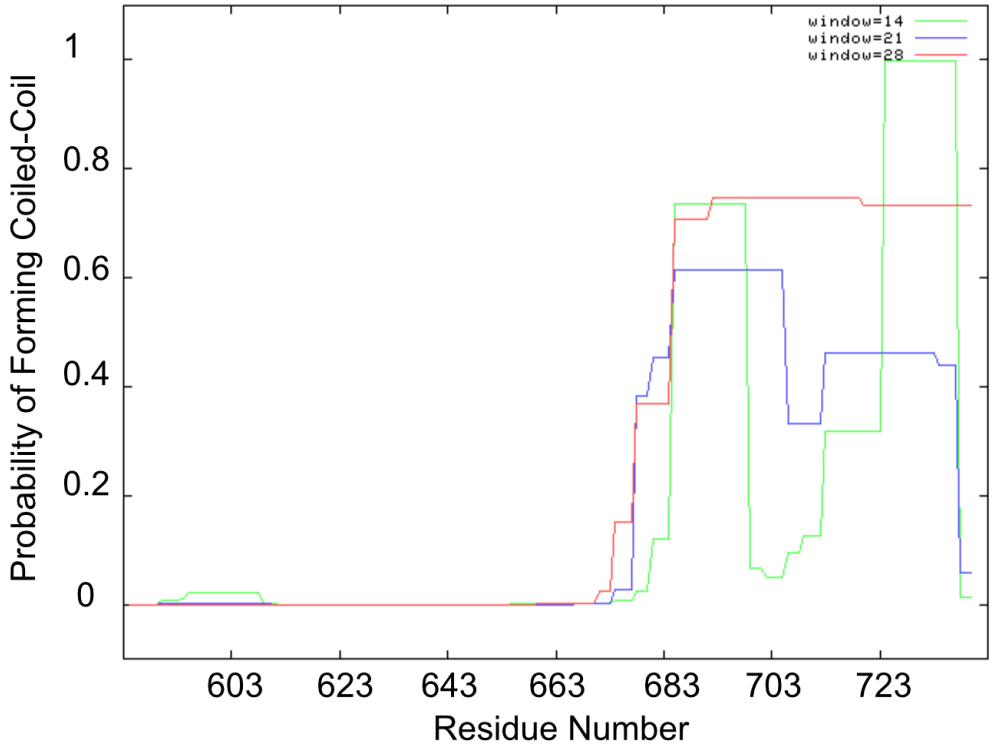

S4 Fig. Coiled-coil prediction of PLPMD. Coiled-coil prediction of PLPMD from the COILS server shows high probability of a coiled coil secondary structure in the carboxyl region of PLPMD.

Supplemental Figure 5 - 2D ^{15}N-HSQC Experiments of Dimeric CM2 in the Presence of CNNLZ and PLPMD

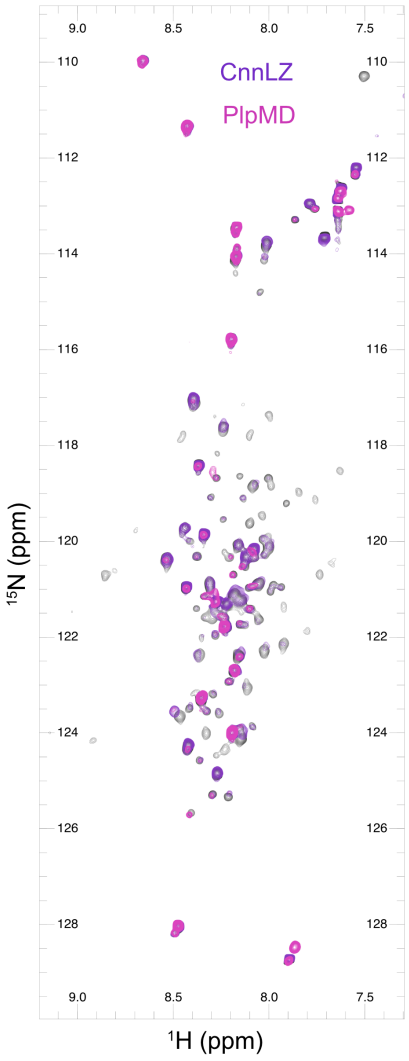

S5 Fig. 2D ^{15}N-HSQC experiments of dimeric CM2 in the presence of CNNLZ and PLPMD. HSQC spectra (gray) of dimeric CM2 with low intensity peaks at lower (<8ppm) proton resonances indicative of multiple species. Overlaid are dimeric CM2 with addition of 75μM CNNLZ (purple) and 100μM PLPMD (pink) that exhibit reduced intensities on a significant number of peaks. All spectra are contoured and scaled identically.

Supplemental Figure 6- 2D ^{15}N-HSQC of Monomeric CM2 in the Presence of Calcium or EGTA

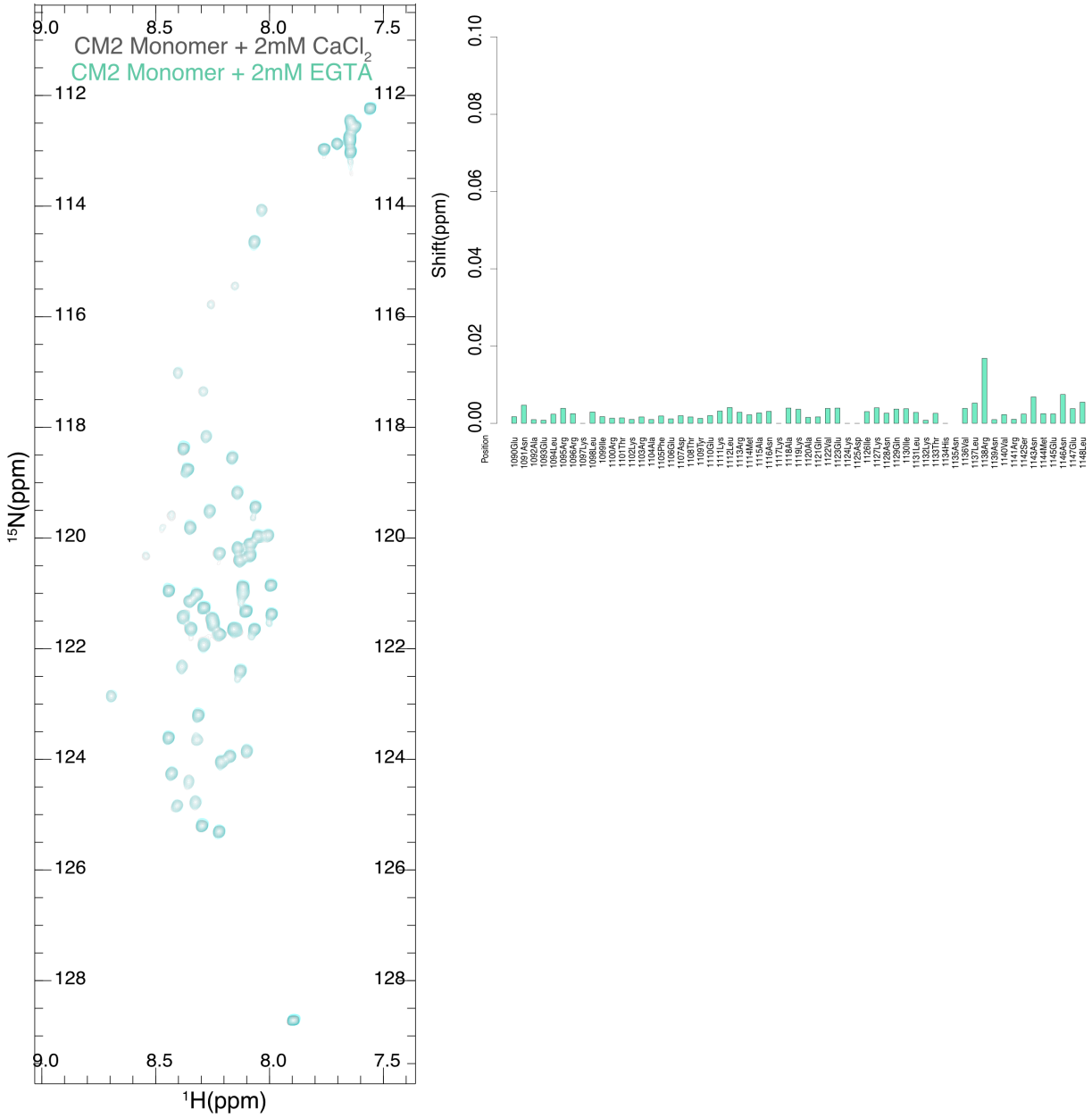

S6 Fig. 2D ^{15}N-HSQC experiments of monomeric CM2 in the presence of 2mM $CaCl_2$ or 2mM EGTA. Overlay of the HSQC spectra of monomeric CM2 in the presence of 2mM $CaCl_2$ (gray) or in the presence of 2mM EGTA (cyan). Visual inspection of the spectra as well as quantification of the combined chemical shifts between the two shows that there are no appreciable difference to the spectra.

Supplemental Figure 7 - 2D ^{15}N-HSQC of dimeric CM2 in the Presence of CaM

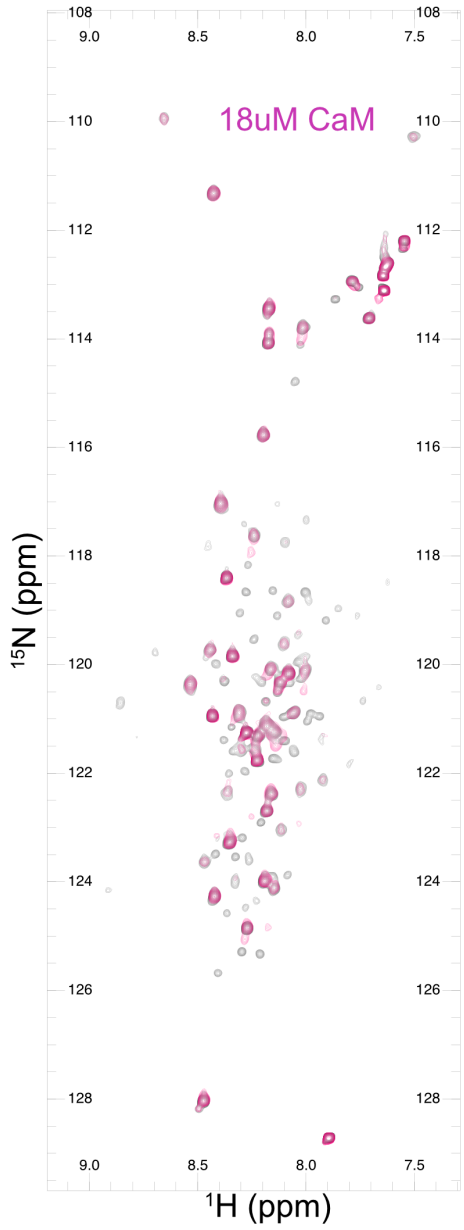

S7 Fig. 2D ^{15}N-HSQC experiments of dimeric CM2 in the presence of CaM. Overlay of the HSQC spectra of dimeric CM2 (gray) and dimeric CM2 with the addition of 18μM CaM (pink) in the presence of 2mM $CaCl_2$. Both spectra are contoured and scaled identically. The intensities of several peaks are reduced dramatically with the addition of CaM and new peaks also appear in the presence of CaM.

Acknowledgments

We thank members of the Huang and Agard lab for helpful discussions. We thank Wei Qiang and Veronica Pessino in the Huang lab for help with cell sorting at various stages of the project. Furthermore, we thank Jeffery G. Pelton for help and access to the Central California 900 NMR facility as well as helpful advice from James Holton at early stages of the project. We thank Jordan Raff for the anti-PLP antibody.

Author Contributions

Conceptualization: Y. Rose Citron, Nasser M. Rusan, David A. Agard.

Data curation: Y. Rose Citron, Carey J. Fagerstrom, Nasser M. Rusan.

Formal analysis: Y. Rose Citron, Bettina Keszthelyi, Nasser M. Rusan, Mark J. S. Kelly.

Funding acquisition: Bo Huang, Nasser M. Rusan, David A. Agard.

Investigation: Y. Rose Citron, Carey J. Fagerstrom, Mark J. S. Kelly.

Methodology: Mark J. S. Kelly.

Resources: Mark J. S. Kelly.

Supervision: Bo Huang, Nasser M. Rusan, David A. Agard.

Writing – original draft: Y. Rose Citron, David A. Agard.

Writing – review & editing: Bo Huang, Nasser M. Rusan, Mark J. S. Kelly, David A. Agard.

References

1. Dobbelaere J, Josue´ F, Suijkerbuijk S, Baum B, Tapon N, Raff J. A Genome-Wide RNAi Screen to Dis- sect Centriole Duplication and Centrosome Maturation in Drosophila. Schliwa M, editor. PLoS Biol. 2008 Sep 16; 6(9):e224. https://doi.org/10.1371/journal.pbio.0060224 PMID: 18798690

2. Megraw TL, Li K, Kao LR, Kaufman TC. The centrosomin protein is required for centrosome assembly and function during cleavage in Drosophila. Development. 1999 Jul; 126(13):2829–39. PMID: 10357928

3. Andersen JS, Wilkinson CJ, Mayor T, Mortensen P, Nigg EA, Mann M. Proteomic characterization of the human centrosome by protein correlation profiling. Nature Publishing Group. 2003 Dec 4; 426 (6966):570–4.

4. Delattre M, Canard C, Go¨nczy P. Sequential Protein Recruitment in C. elegans Centriole Formation. Current Biology. 2006 Sep; 16(18):1844–9. https://doi.org/10.1016/j.cub.2006.07.059 PMID: 16979563

5. Mennella V, Keszthelyi B, McDonald KL, Chhun B, Kan F, Rogers GC, et al. Subdiffraction-resolution fluorescence microscopy reveals a domain of the centrosome critical for pericentriolar material organization. Nature Cell Biology. Nature Publishing Group; 2012 Oct 21; 14(11):1159–68.

6. Fu J, Glover DM. Structured illumination of the interface between centriole and peri-centriolar material. Open Biology. 2012 Aug 1; 2(8):120104–4. https://doi.org/10.1098/rsob.120104 PMID: 22977736

7. Lawo S, Hasegan M, Gupta GD, Pelletier L. Subdiffraction imaging of centrosomes reveals higher- order organizational features of pericentriolar material. Nature Cell Biology. Nature Publishing Group; 2012 Oct 21; 14(11):1148–58.

8. Woodruff JB, Gomes BF, Widlund PO, Mahamid J, Honigmann A, Hyman AA. The Centrosome Is a Selective Condensate that Nucleates Microtubules by Concentrating Tubulin. Cell. Elsevier Inc; 2017 Jun 1; 169(6):1066–1071.e10.

9. Galletta BJ, Fagerstrom CJ, Schoborg TA, McLamarrah TA, Ryniawec JM, Buster DW, et al. A centrosome interactome provides insight into organelle assembly and reveals a non-duplication role for Plk4. Nature Communications. Nature Publishing Group; 2016 Aug 17; 7:1–15.

10. Choi Y-K, Liu P, Sze SK, Dai C, Qi RZ. CDK5RAP2 stimulates microtubule nucleation by the γ-tubulin ring complex. J Cell Biol. 2010 Dec 13; 191(6):1089–95. https://doi.org/10.1083/jcb.201007030 PMID: 21135143

11. Hamill DR, Severson AF, Carter JC, Bowerman B. Centrosome maturation and mitotic spindle assembly in C. elegans require SPD-5, a protein with multiple coiled-coil domains. Developmental Cell. 2002 Nov; 3(5):673–84. PMID: 12431374

12. Buchman JJ, Tseng H-C, Zhou Y, Frank CL, Xie Z, Tsai L-H. Cdk5rap2 Interacts with Pericentrin to Maintain the Neural Progenitor Pool in the Developing Neocortex. Neuron. Elsevier Ltd; 2010 May 13; 66(3):386–402.

13. Wang Z, Wu T, Shi L, Zhang L, Zheng W, Qu JY, et al. Conserved Motif of CDK5RAP2 Mediates Its Localization to Centrosomes and the Golgi Complex. J Biol Chem. 2010 Jul 9; 285(29):22658–65. https://doi.org/10.1074/jbc.M110.105965 PMID: 20466722

14. Lerit DA, Jordan HA, Poulton JS, Fagerstrom CJ, Galletta BJ, Peifer M, et al. Interphase centrosome organization by the PLP-Cnn scaffold is required for centrosome function. J Cell Biol. 2015 Jul 6; 210 (1):79–97. https://doi.org/10.1083/jcb.201503117 PMID: 26150390

15. Feng Z, Caballe A, Wainman A, Johnson S, Haensele AFM, Cottee MA, et al. Structural Basis for Mitotic Centrosome Assembly in Flies. Cell. Elsevier Inc; 2017 Jun 1; 169(6):1078–1083.e13.

16. Zhang J, Megraw TL. Proper Recruitment of γ-Tubulin and D-TACC/Msps to Embryonic Drosophila Centrosomes Requires Centrosomin Motif 1. Molecular Biology of the Cell 2007 Sep 17;:1–13.

17. Samejima I, Miller VJ, Groocock LM, Sawin KE. Two distinct regions of Mto1 are required for normal microtubule nucleation and efficient association with the γ-Tubulin complex in vivo. Journal of Cell Sci- ence. 2008 Nov 19; 121(23):3971–80.

18. Rogers GC, Rusan NM, Roberts DM, Peifer M, Rogers SL. The SCF Slimbubiquitin ligase regulates Plk4/Sak levels to block centriole reduplication. J Cell Biol. 2009 Jan 26; 184(2):225–39. https://doi.org/ 10.1083/jcb.200808049 PMID: 19171756

19. Rhoads AR, Friedberg F. Sequence motifs for calmodulin recognition. FASEB J. 1997 Apr; 11(5):331– 40. PMID: 9141499

20. Richens JH, Barros TP, Lucas EP, Peel N, Pinto DMS, Wainman A, et al. The Drosophila Pericentrin- like-protein (PLP) cooperates with Cnn to maintain the integrity of the outer PCM. Biology Open. 2015 Aug 15; 4(8):1052–61. https://doi.org/10.1242/bio.012914 PMID: 26157019

21. Brownlee CW, Klebba JE, Buster DW, Rogers GC. The Protein Phosphatase 2A regulatory subunit Twins stabilizes Plk4 to induce centriole amplification. J Cell Biol. 2011 Oct 17; 195(2):231–43. https:// doi.org/10.1083/jcb.201107086 PMID: 21987638

22. Ball G, Demmerle J, Kaufmann R, Davis I, Dobbie IM, Schermelleh L. SIMcheck: a Toolbox for Suc- cessfulSuper-resolution StructuredIllumination Microscopy. Nature Publishing Group. Nature Publishing Group; 2015 Oct 29;:1–11.

23. Delaglio F, Grzesiek S, Vuister GW, Zhu G, Pfeifer J, Bax A. NMRPipe: a multidimensional spectral pro- cessing system based on UNIX pipes. J Biomol NMR. 1995 Nov; 6(3):277–93. PMID: 8520220

24. Schubert M, Smalla M, Schmieder P, Oschkinat H. MUSIC in triple-resonance experiments: amino acid type-selective (1)H-(15)N correlations. J Magn Reson. 1999 Nov; 141(1):34–43. https://doi.org/10. 1006/jmre.1999.1881 PMID: 10527741

25. Vranken WF, Boucher W, Stevens TJ, Fogh RH, Pajon A, Llinas M, et al. The CCPN data model for NMR spectroscopy: Development of a software pipeline. Proteins. 2005 Apr 6; 59(4):687–96. https:// doi.org/10.1002/prot.20449 PMID: 15815974

26. Hajduk PJ, Dinges J, Miknis GF, Merlock M, Middleton T, Kempf DJ, et al. NMR-based discovery of lead inhibitors that block DNA binding of the human papillomavirus E2 protein. J Med Chem. 1997 Sep 26; 40(20):3144–50. https://doi.org/10.1021/jm9703404 PMID: 9379433

Chapter III – Characterization of CM2 dimerization and dimer species.

Introduction

As described in the previous section, CM2 was found to be dimeric but the minimal domain and exact residues that mediate this dimerization were not examined. In this chapter, I describe experiments preformed in order to better identify the mechanism of dimerization. Furthermore, I describe a number of experiments designed and executed in order to better understand the role of zinc in dimerization in response to the report from Feng et. al. [1] that zinc may play an important role in dimerization.

Understanding the mechanism and species of dimeric CM2 is of relevance for a number of reasons. Firstly, to establish if the dimer is mediated through canonical coiled-coil interactions and if not, to better understand how this interaction occurs. The nature of dimerization may also be a point regulation as implied if the zinc is a requirement for dimerization. Additionally, dimerization of CM2 and more generally the multivalency of centrosomin has implications in understanding the general properties assembly and behavior of protein in the centrosome.

Results and Discussion

As described in chapter one two dimeric constructs were characterized with SEC-MALS – aa1064-1148 and aa1074-1148. The first, aa1064-1148, was used for in cell experiments while the second, aa1074-1148, has ten amino terminus residues trimmed off and is used in experiments described in this chapter as minimal domain for dimer characterization. This construct is referred to as wild-type dimeric CM2 for the remainder of this chapter.

The first characterization of the wild type dimer was to crudely test the affinity of the interaction by diluting the protein and running SEC-MALS to observe if a monomer peak appeared at low concentrations. This was in fact not the case, as even when diluted approximately 5 fold to 0.58uM on the SEC-MALS column the protein migrated on the gel filtration column equivalently to protein at 3.2uM (Fig 1A). Furthermore, the molecular weight was comparable regardless of the concentration with a calculated of molecular weight of 19.3kDa at 0.58uM and 19.2kDa at 3.2uM (the predicted molecular weight of a monomer is 8.6kDa). Though this affinity estimate was useful for designing and evaluating further experiments, future work should more rigorously quantify the wild-type dimer affinity using AUC.

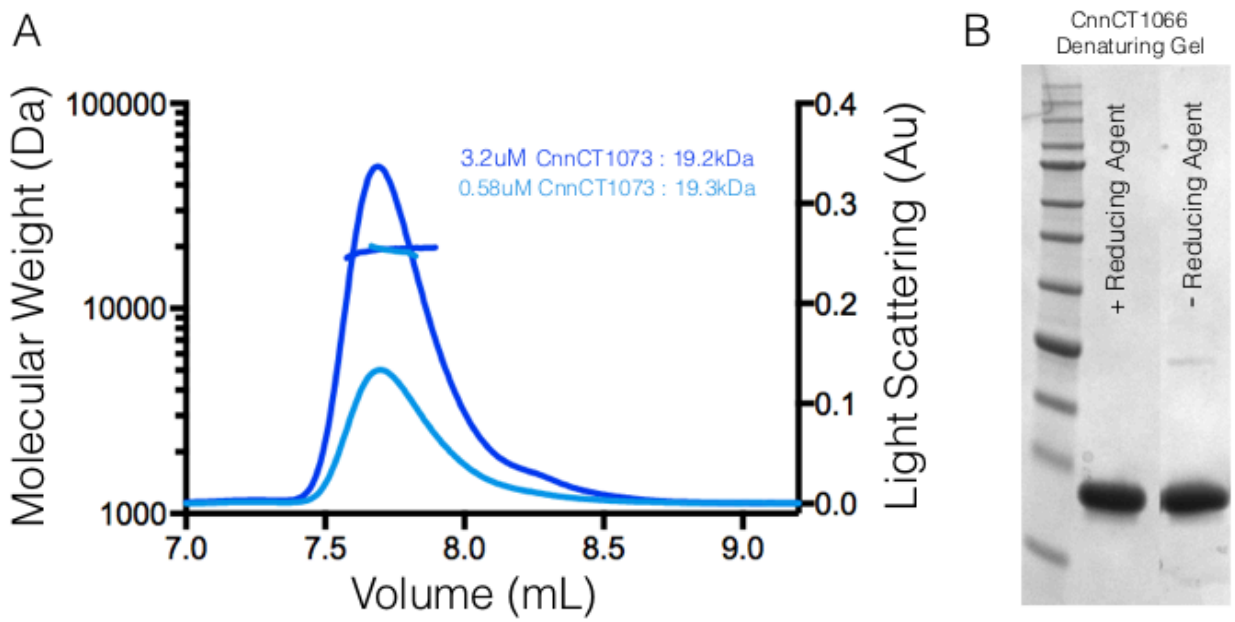

Fig 1. CM2 aa 1074-1148 forms a non-covalent high affinity dimer. (A) SEC-MALS of 3.2uM and 0.58uM wild-type CM2 showing similar profiles and similar molecular weight calculations. (B) A denaturing gel of CM2 with and without reducing agent shows similar protein bands in both conditions. There is no significant dimer band in the absence of reducing agent negating the possibility of a disulfide bridge dimer.

Next, I investigated in greater detail the specific regions and residues of CM2 that contribute to dimerization. Because CM2 contains a single cysteine I sought to test if a disulfide bridge linked the monomers into a dimer by running a 10% bis-tris acrylamide denaturing gel and comparing protein with and without reducing agent in SDS loading buffer. Both with and without reducing agent (2-Mercaptoethanol) CM2 ran as expected for a monomer (Fig 1B). A weak dimer band was visible in the absence of reducing agent, however, this does not make up a significant population of the total protein. This data indicates that a cysteine disulfide bridge is not the driving biochemical interaction that dimerizes CM2 instead indicating another mechanism.

To evaluate the residues involved in dimerization further, alanine mutations were made in and run on SEC-MALS to assess the oligomerization state. Given that the truncated CM2 construct aa1090-1148 is monomeric, we were able to narrow down the dimerization region to small stretch of residues and design alanine mutations along this length of amino acids (Fig 2A). The mutants illustrated in figure 2A were purified and run on SEC-MALS. As seen in figure B, CnnCT 1074 TV/AA remains predominately dimeric though a small monomer shoulder exists while CnnCT 1074 HDC/AAA is exclusively monomeric at equivalent concentrations. To narrow down the individual residues CnnCT 1074 H/A and CnnCT 1074 D/A constructs were run on SEC-MALS and showed that both mutations disrupt the monomer-dimer equilibrium to similar extents as both monomer and dimer peaks appear on SEC-MALS. Importantly, circular dichroism was performed on the point mutants CnnCT 1074 H/A and CnnCT 1074 D/A and compared to wild-type dimeric CM2 (Fig 2D). Circular dichroism profiles for all three protein constructs are typical of helical secondary structure showing that the single point mutants do not

monomerize the dimer by profoundly disrupt the fold. Given this data and specifically the information that a histidine was involved in mediating dimerization, we reasoned that dimerization may be dependent on the protonation state of the histidine making it pH sensitive.

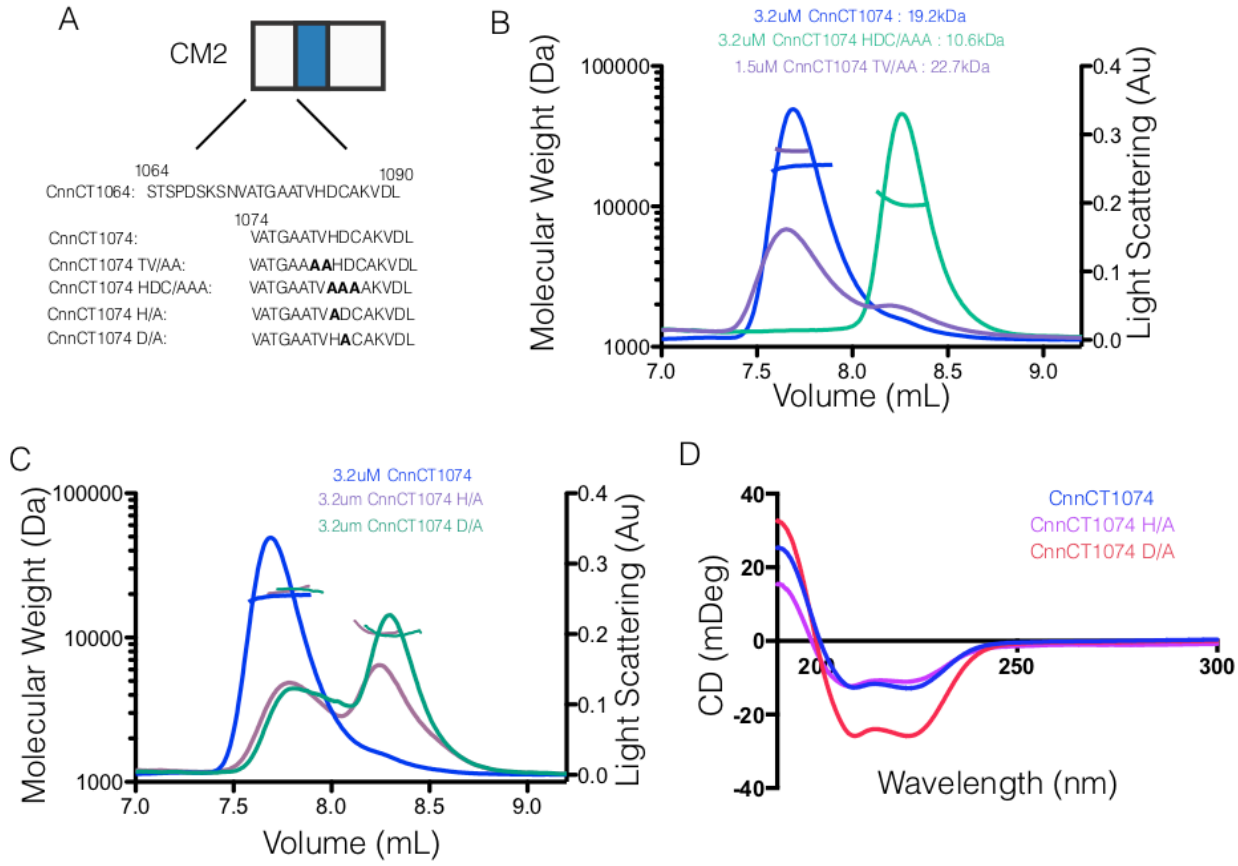

Fig 2. SEC-MALS of CM2 alanine mutations identifies key residues. (A) Schematic of different constructs of CM2. Comparison of dimeric CM2 aa1074-1148 and monomeric CM2 aa1090-1148 narrows down the region responsible for dimerization to a stretch of 16 residues. Alanine mutations were designed in this area of residues to further pin point dimerization. (B) Comparison of SEC-MALS profiles of wildtype CM2 with CM2 TV/AA and CM2 HDC/AAA. CM2 TV/AA remains predominately dimeric despite being at ~50% the concentration of the wildtype CM2. On the other hand, CM2 HDC/AAA is entirely monomeric despite being at equivalent concentrations to wildtype CM2. (C) Single point alanine mutations in the CM2 HDC/AAA region. Both CM2 H/A and D/A constructs are mixture of monomer and dimer species at concentrations similar to wildtype CM2. (D) Circular dichroism of wild-type dimeric CM2 (blue) compared to CM2 H/A (purple) and D/A (pink) shows that all constructs are typical of helical secondary structure. Changes in the intensity of y-axis are reflective only of the protein concentration while the relative ratios of peaks and valleys are indicative of secondary structure content.

In order to test if the protonation state of this histidine was important, wild-type dimeric CM2 was run on SEC-MALS at pH 5.8 and compared it with SEC-MALS at pH 8.0. As a control for the proper function of the SEC-MALS instrumentation, I ran bovine serum albumin (BSA) at each pH. I note that for the control the molecular weight determination is identical at pH 5.8 and 8.0 (68kDa), however, that elution volume is slightly shifted between the different pHs (Fig 3A).

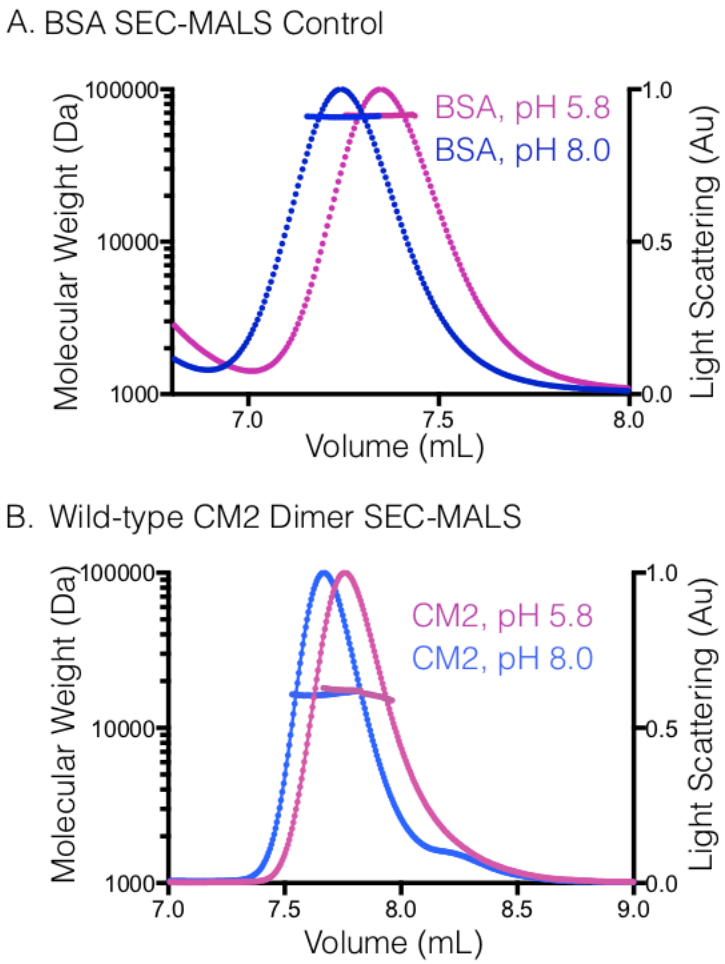

Fig 3. SEC-MALS of wild-type dimeric CM2 at pH 5.8 and 8.0. (A) A BSA control with running buffer pHed to 5.8 (pink) and 8.0 (blue) run on SEC-MALS. Though there is a pH dependent shift in the elution volume, the molecular weight determination is equivalent at both high and low pH and gives a reasonable molecular weight of 68.0kDa. (B) SEC-MALS of wild-type dimeric CM2 in running buffer pHed to 5.8 (pink) and 8.0 (blue). At both pHs the protein runs with a predominate dimeric peak, with molecular weight calculations of 18.1kDa. A small monomer shoulder (10kDa) appears at high pH.

The expectation is that this is a result of a pH dependent interaction with column resin though I did not investigate further. Next, the exact same wild-type dimeric CM2 sample was run on SEC-MALS with running buffers pHed to 5.8 and 8.0 (Fig3B). While the same elution volume shift that is seen in the control is seen with wild-type dimeric CM2, the predominate peak remains dimeric at both low (5.8) and high (8.0) pH. Interestingly, a small shoulder that may correspond to a monomer population appears at high pH, indicating that perhaps at slightly higher pH the dimer may become disrupted. This suggests a potential mechanism of dimerization where a positive charge on the histidine interacts through a salt bridge. In particular, if this region of the protein is forming a helix the positively charged histidine on one monomer arm maybe forming a salt bridge with the aspartic acid on the second monomer (Fig 4A).

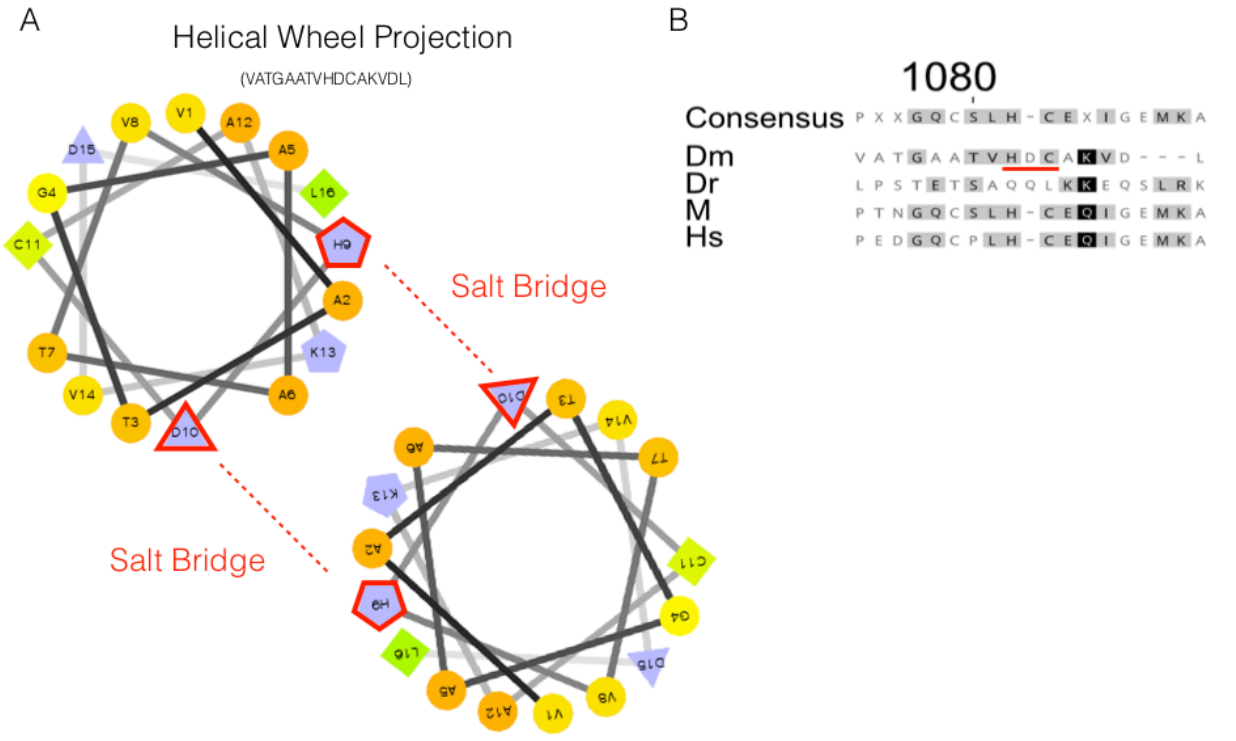

Fig 4. Helical wheel projection of wild-type CM2 shows a potential mechanism of interaction. (A)The helical wheel projection of the required region for dimerization (VATGAATVHDCAKVDL) shows a potential mechanism whereby the histidines (outlined in

red pentagons) on opposite monomers are positioned to form salt bridges with aspartic acids (outlined in red triangles). (B) Sequence alignment of the required region for dimerization (VATGAATVHDCAKVDL) shows the HDC amino acids (underlined in red) are not conserved in zebra fish and that only histidine and cysteine are conserved in mouse and human homologues.

At high pH, when the positive charge on the histidine is lost, this salt bridge maybe disrupted and monomerize the dimer. This possibility should be further explored in the future by repeating the SEC-MALS experiments but in even higher pHs. Additionally, SEC-MALS in the presence of high salt could help bolster this hypothesis as well as repeating these experiments using AUC to better quantitate the affinities under different conditions. One argument against such a mechanism is the conservation of these residues in other organisms (Fig 4B). Though the histidine and nearby cysteine are conserved in mouse and human homologues, the aspartic acid is not conserved. Given the assumption that all CM2 homologues form dimers, either this suggested mechanism is not accurate or different homologues have developed distinct methods for dimerization.

Another proposed mechanism of dimerization was put forward by data published by Feng et. al. [1]. In this work they solve a number of crystal structures and find a zinc atom in the dimer interface and specifically coordinated by histidine and cysteine (Fig 5A) – the specific set of residues identified previously in this chapter as being important for dimerization using SEC-MALS. Furthermore, SEC-MALS experiments performed by the Raff group shows, consistent with the above described data, that CnnCT 1074 HDC/ADA is monomeric (Fig 5B) and that wild-type CM2 dimer treated with EDTA to chelate zinc is monomeric (Fig 5B). In response to t these data, numerous experiments were preformed to better understand if these reports were consistent with our data and try to better understand the context of when this zinc interaction is physiologically meaningful.

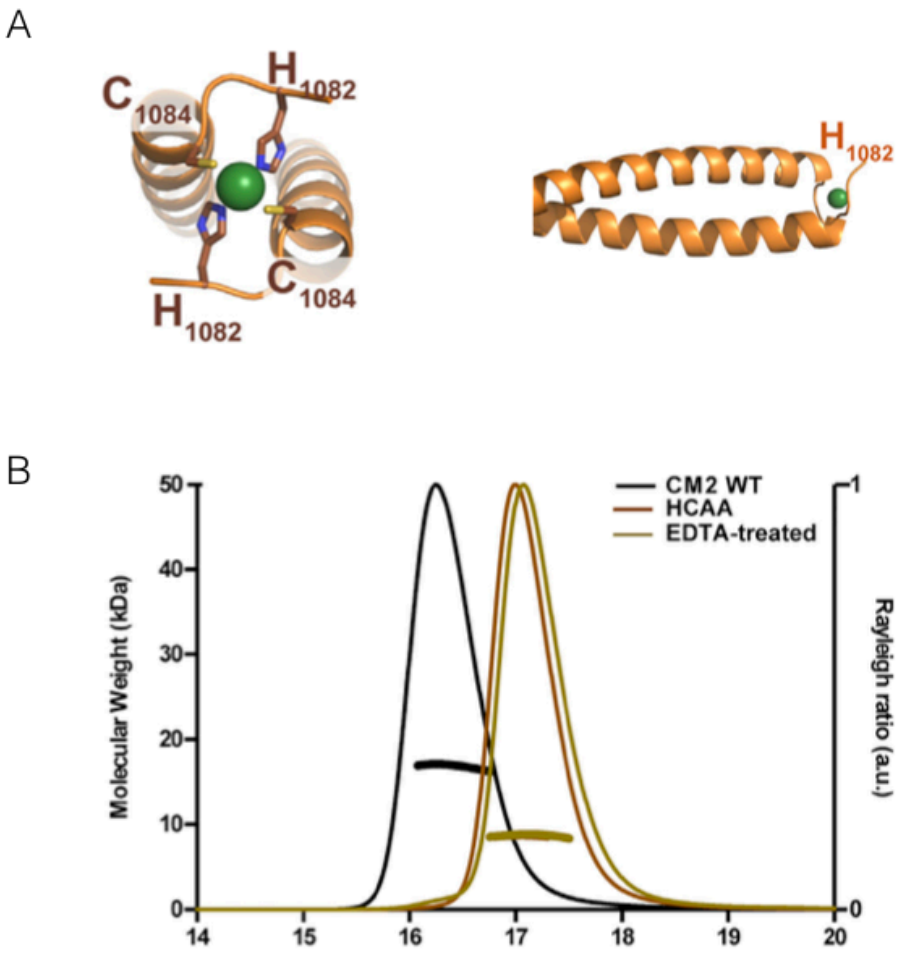

Fig 5. Crystal structures of CM2 contain zinc atom coordinated by histidine and cysteine. (A) Adapted figures from Feng et. al. show a zinc atom (green) coordinated by CM2 (orange) and specifically by histidine 1082 and cysteine (1084). (B) SEC-MALS of wild-type dimeric CM2 compared to CnnCT 1074 HDC/ADA and EDTA treated wild-type CM2 preformed and published by the Raff lab.

Firstly, I tried to reproduce the Raff lab result whereby EDTA incubation monomerized wild-type CM2. In order to do this, I dialyzed wild-type dimeric CM2 into buffer containing 2mM EDTA overnight and then ran in the sample on SEC-MALS equilibrated into the same EDTA containing buffer. The result was the appearance of a monomer peak (10.4kDa), however, a strong dimer peak remained (25.4kDa) despite the presence of EDTA and the relatively low concentration of 0.37uM on the column (Fig 6). My inability to reproduce the published results

may stem from a number of issues, though it is worth noting that EDTA does in fact affect dimerization in my experiments but not to the extent seen in the published data. No protein concentration is listed in the published data and the Rayleigh ratio is normalized to 1, therefore, it is possible that the published results were run at lower concentrations which would shift the predominate peak to monomer. Another possibility for the discrepancy may be the difference in wild-type CM2 constructs. The construct in my experiments contains an additional eight amino terminal residues compared to that used in the published work. These additional residues likely contribute some affinity given that CnnCT 1074 TV/AA, though mostly dimer, has a small monomer shoulder on SEC-MALS (Fig 2B).

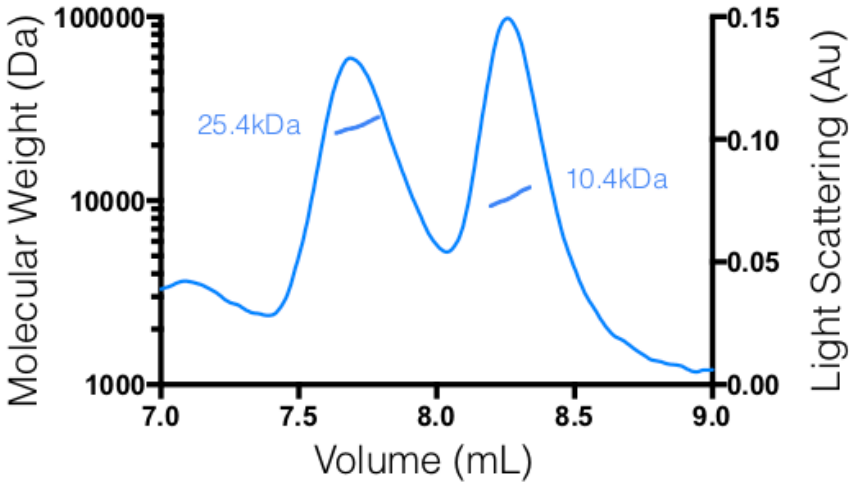

Fig 6. SEC-MALS of EDTA treated wild-type CM2. Wild-type dimeric CM2 was dialyzed into 2mM EDTA containing buffer and run on SEC-MALS. The results show that 50-60% of the protein becomes monomeric (10.4kDa) showing that zinc or another cation contributes some affinity to dimerization.

To better understand the effects of zinc and chelating agents on wild-type dimeric CM2, various NMR spectra were recorded and compared under different conditions. In the context of trying to understand the calcium sensitivity of CM2's interaction with calmodulin, N^{15} isotope

labeled wild-type CM2 dimer ie. CnnCT 1074, was dialyzed into two buffers - one containing additional 2mM $CaCl_2$ and one containing additional 2mM EGTA. Though EDTA is better chelator of zinc, EGTA chelates zinc to a lesser degree. HSQC spectra of each sample with 50uM protein was recorded and chemical shifts overlaid for comparison. While CM2 in the presence of $CaCl_2$ was reminiscent of monomeric CM2 HSQC spectra, the spectra of CM2 treated with 2mM EGTA was significantly perturbed (Fig 7A). In the presence of EGTA, numerous chemical shifts disappeared, appeared and were shifted relative to CM2 with $CaCl_2$. These significant changes in the spectra suggest that there is a change in the conformation of each monomer structure, a change in the oligomer state or both. Given that no such changes are seen in the monomeric version of CM2 under calcium and EGTA conditions (see chapter II, supplemental figure 6), these data indicate that any changes that are occurring in the context of CnnCT 1074 are driven by the additional 16 amino terminus residues.

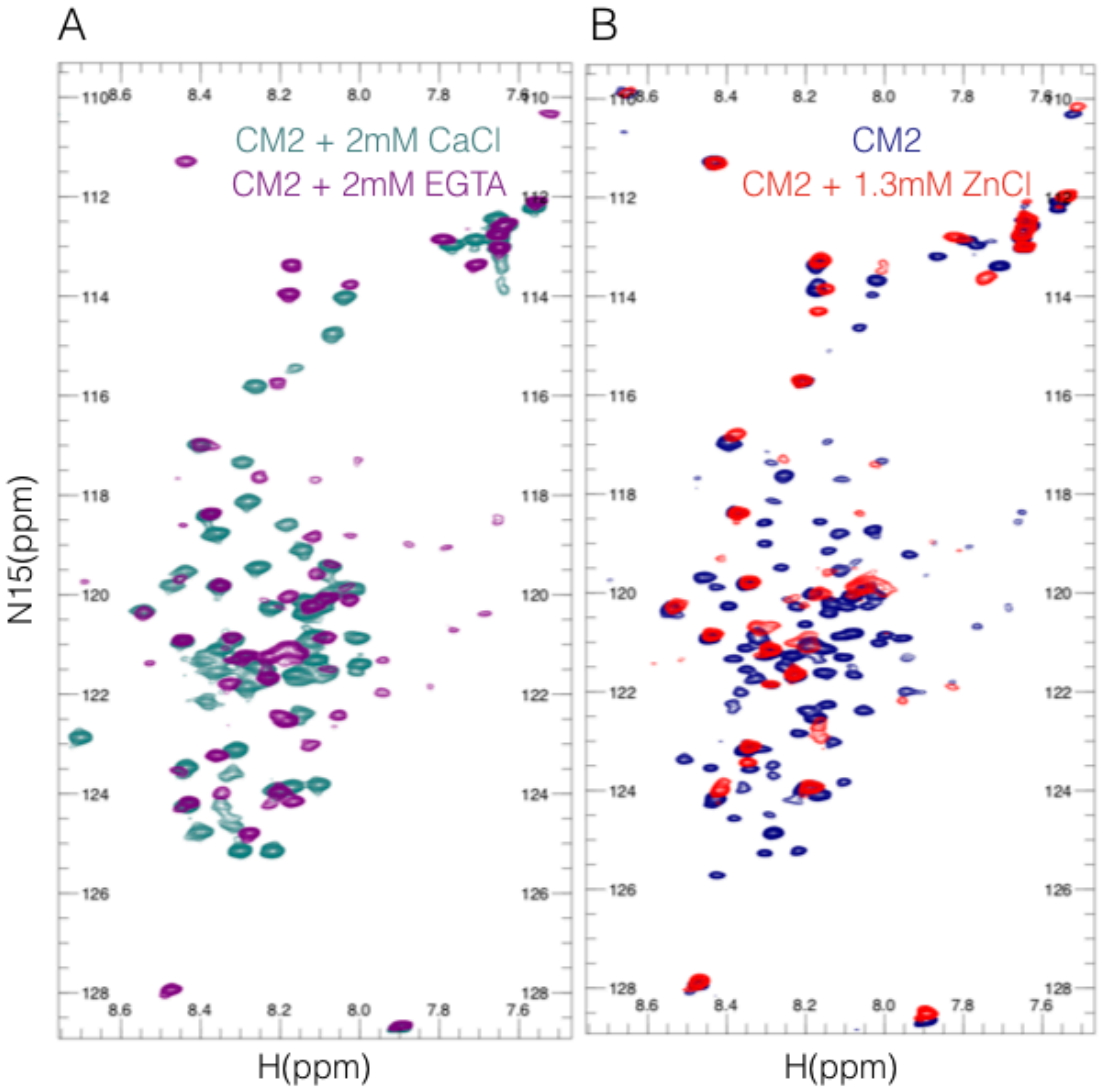

Fig 7. Presence of zinc or chelating agent significantly changes HSQC spectra of wild-type dimeric CM2. (A) Comparison of HSQC spectra of 50uM wild-type dimeric CM2 in the presence of 2mM $CaCl_2$ (teal) or the presence of 2mM EGTA (purple). While the presence of calcium yields spectra that is similar to monomeric CM2 spectra, numerous chemical shifts disappear, shift, and appear in the presence of EGTA. (B) Comparison of HSQC spectra of 50uM wild-type dimeric CM2 alone (blue) and upon addition of 1.3mM $ZnCl_2$ (red). Before addition of zinc, the CM2 spectra looks similar to monomeric CM2 spectra, but upon addition of zinc numerous peaks disappear. Note: None of the spectra in (A) should be directly compared to the spectra in (B) as these spectra were collected in different buffers of slightly different pH and different batches of labeled protein.

In an attempt to understand if chelation of the zinc is what led to these profound changes, another set of experiments were preformed where HSQC spectra were recorded before and after spiking in 1.3mM $ZnCl_2$ (Fig 7B). Again, significant changes are seen between the chemical shifts of CM2 with and without zinc and specifically the presence of zinc results in a significant loss of chemical shifts. One possible explanation of these data is that addition of zinc results in the formation of higher order species with increased tumbling time which in turn results in broaden chemical shifts that are no longer visible. To check if this is the case, a TROSY spectra of the same sample was recorded (Fig 8). Though a couple weak peaks are recovered, there is not the appearance of a significant number of peaks nor do those weak peaks correspond to any of the chemical shifts lost upon addition of zinc.

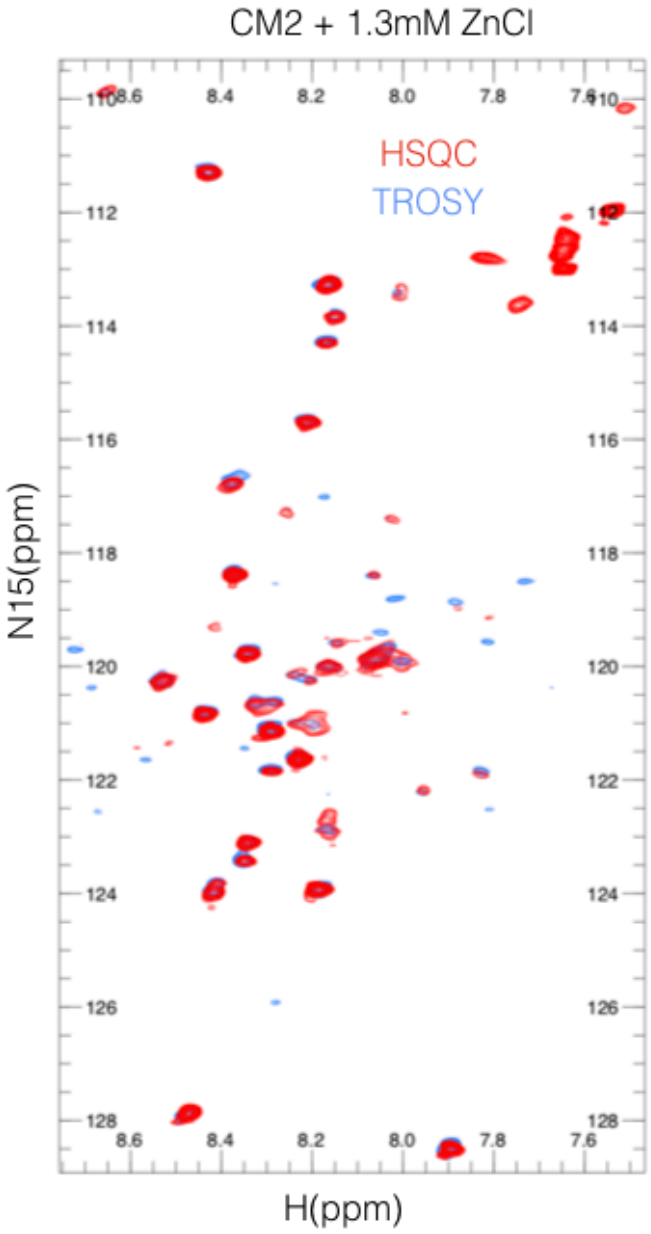

Fig 8. TROSY spectra of zinc treated CM2 suggests that zinc does not induce higher order species. Comparison of an HSQC (red) and TROSY (blue) spectra on wild-type CM2 (CnnCT 1074) in presence of 1.3mM $ZnCl_2$. Though a few weak chemical shifts are visible in the TROSY, there is not a significant difference in the spectra indicating the disappearance of chemical shifts upon addition of zinc is not due to large oligomer species.

Overall, the NMR data comparing different conditions to illuminate the role of zinc in mediating dimerization is puzzling. The significant change in chemical shifts in the presence of EGTA that occurs only in dimeric construct indicates a profound change along the length of protein that is driven by amino terminus residues interacting with zinc or calcium. Yet, if the predominate species of dimeric CM2 was bound to zinc, one would not expect to see the massive chemical shift changes upon addition of 1.3mM zinc. One explanation maybe that numerous dimeric species exist as described in chapter II (supplemental figure 2), the predominate one being reminiscent of the monomeric species by NMR. The presence or absence of cations, calcium or zinc, shifts the exchange rate between various dimeric and monomeric species such that they are no longer in intermediate exchange and therefore invisible by HSQC spectra. This may also explain why the spectra of CM2 with the addition of 2mM EGTA and with 1.3mM $ZnCl_2$ look somewhat similar. If both of these additions shift the equilibrium, the peaks that remain may simply be the strongest peaks of predominate species.

Despite extensive studies that give hints at two potential types of protein-protein interactions mediating CM2 dimerization, the mechanism of this dimerization is still unclear. On the one hand, a salt bridge between histidine 1082 and aspartic acid 1083 on the opposite monomer may be responsible for dimerization. On the other hand, published data and original data presented in the chapter suggest that chelating agents and the presence of zinc or calcium alter the protein conformation or oligomer state. Both mechanisms are potentially surprising given that sequence required to achieve them is not conserved in other metazoan species and may mean that distinct mechanisms have evolved for dimerization. Or potentially more interestingly, that other species do not have dimeric CM2. Future work, should continue to explore these mechanisms. Likely the most fruitful experiments will be the use of AUC to more

quantitatively characterize the affinity contributions of individual residues and different cations to dimerization. Additionally, AUC will be able to provide information about numerous conformational species and how these may shift under different conditions.

Materials and methods

Protein expression and purification

Labeled and native proteins were cloned, expressed and purified as described in chapter II's materials and methods section.

SEC-MALS

Multi-angle light scattering analysis was performed with a KW-802.5 size exclusion column on an Ettan liquid chromatography system (GE Healthcare Life Sciences) with inline DAWN HELEOS MALS and Optilab rEX differential refractive index detector (Wyatt Technology). All samples were in 50mM HEPES pH 7.0, 200mM NaCl, and 1mM DTT running buffer except in the case of the low and high pH testing. These experiments were run 50mM sodium phosphate buffer, 150mM NaCl and 1mM DTT and then pHed either to 5.8 or 8.0 as specified in the text. Data were analyzed using ASTRA VI system software (Wyatt Technology).

Nuclear magnetic resonance

All 2D [^{15}N, ^{1}H]-HSQC (pulse program: fhsqcf3gpph) binding experiments were carried out with 50μM of ^{15}N labeled protein on an 800 MHz Bruker AVANCEI spectrometer. HSQC experiments were performed at 300K with all proteins dialyzed overnight into 20mM PIPES pH

6.8, 140mM NaCl, 0.01% (w/v) NaN_3, 5% (v/v) D_2O with the addition of either 2mM $CaCl_2$, 2mM EGTA or 2mM $ZnCl_2$. Analysis was done in CCPNMR [2].

References

1. Feng Z, Caballe A, Wainman A, Johnson S, Haensele AFM, Cottee MA, et al. Structural Basis for Mitotic Centrosome Assembly in Flies. Cell. Elsevier Inc; 2017 Jun 1; 169(6):1078–1083.e13.
2. Vranken WF, Boucher W, Stevens TJ, Fogh RH, Pajon A, Llinas M, et al. The CCPN data model for NMR spectroscopy: Development of a software pipeline. Proteins. 2005 Apr 6; 59(4):687–96. https:// doi.org/10.1002/prot.20449 PMID: 15815974

Chapter IV – X-Ray Crystallography and Structural Studies of CM2

Introduction

In order to fully understand CM2, how if functions as scaffold in centrosome and how it is regulated, numerous attempts were made to gain an atomic level structure of CM2. Unfortunately, prior to these attempts being fruitful a structure was published by the Raff lab [1] such that this line of experimentation was not finished. In this chapter, I will describe the numerous experiments preformed to characterize the structure of CM2, the information that we gain from these data, and how they can be interpreted in light of the Raff lab structure.

Results and Discussion

Beyond characterizing the oligomer state of CM2, the first and most basic structural characterization that was performed on CM2 was collecting small angle X-ray scattering (SAXS) data. Data was collected to compare dimeric CM2 (aa1064-1148) with monomeric CM2 (aa1090-1148). Both these proteins exhibit highly extended structures with maximum dimensions of 103Å and 66Å, respectively. Furthermore, using custom software written by Daniel Elnatan based on previously published theory [2] molecular weights were calculated as 24kDa for dimeric CM2 and 9kDa for monomeric CM2. These values are extremely consistent with the molecular weights determined by multi-angle light scattering described in chapter II (22.4kDa and 7.4kDa).

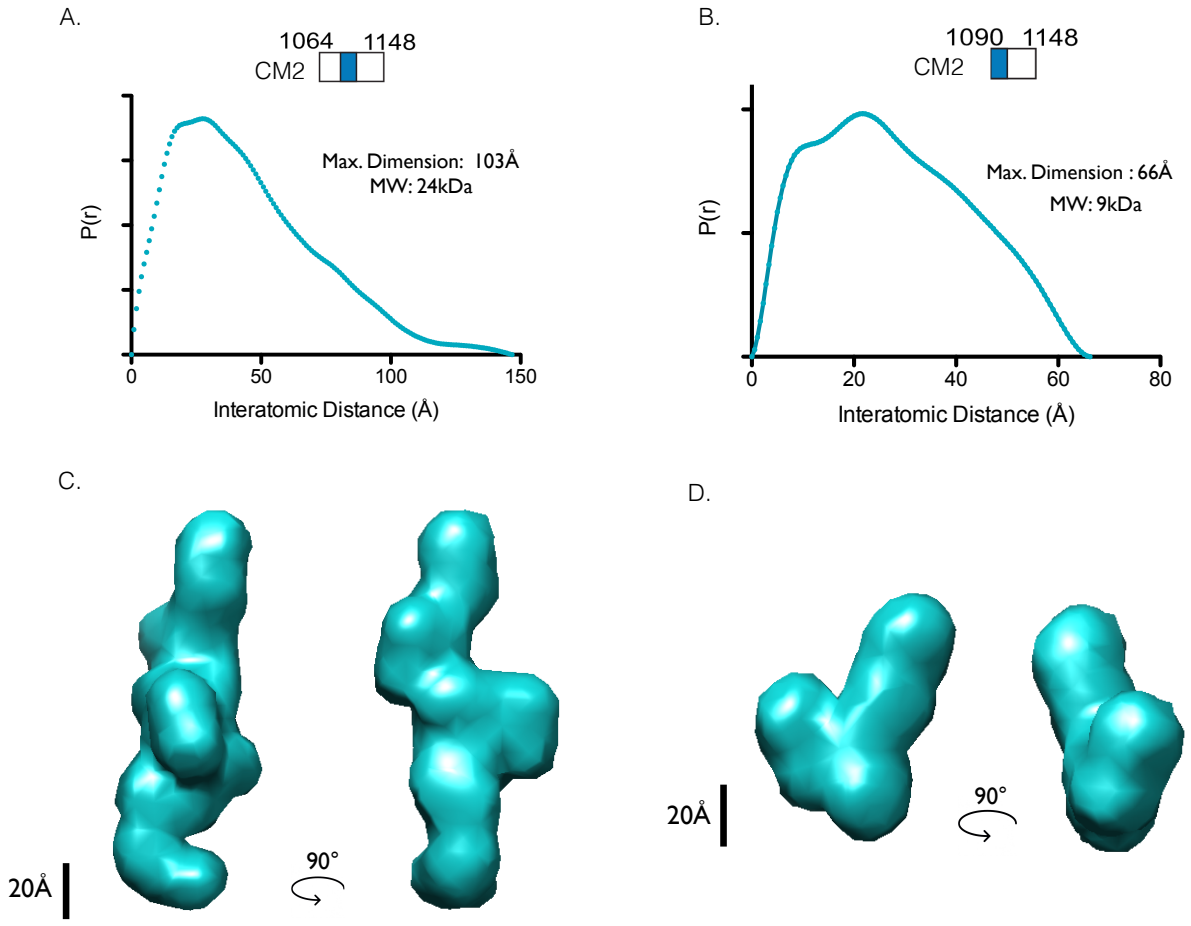

Figure 1. SAXS data of dimeric and monomeric CM2 shows elongated structure. (A) SAXS shows a highly extended conformation of dimeric CM2 with a maximum dimension of 103 Å. (B) SAXS data of monomeric CM2 again shows a highly extended structure with a maximum dimension of 66 Å. (C) A model built using SAXS data for the dimer and (D) monomer.

Additionally, *ab initio* modeling was performed on these SAXS data sets. These models have some interesting features. For dimeric CM2, we initially noted that the model does not exhibit a symmetric structure as would be expected for a symmetric dimer. Because we know there are multiple conformations of dimeric CM2 (see chapter II and III), these data are capturing and adding multiple species as single bulk measurement. Therefore, though the maximum dimension is an accurate average for all species, the model generated likely does not represent any one conformation of dimeric CM2. For monomeric CM2, on the other hand, we have no

evidence of multiple species and the features seen are likely fairly accurate. The main lobe likely corresponds to the main helix while the secondary lobe alongside it maybe the final residues which are unstructured and do not appear in the crystal structure.

It is worth noting, that the Guinier plot for both monomeric and dimeric CM2 indicate monodispersion of the proteins (data not shown). For the monomer this is important as it indicates that even at concentrations greater than 500uM (data was collected at 4mg/ml), the protein remains monomeric. This gives confidence in interpreting previously described in-cell and NMR experiments done with the monomeric construct (aa1090-1148) as being truly monomeric despite relatively high or unknown concentrations.

Though the SAXS data provided insightful information about the shape of CM2, I sought to gain an atomic level structure using x-ray crystallography. To so I started with the aa1064-1148 dimeric CM2 construct. Initial crystallography trays were set with ~5.6mg/ml of protein at room temperature using the Qiagen JCSG Suites I, II, III, and IV as well as the Classical Suite I and II. Crystals formed in these screens were confirmed to be protein by x-ray diffraction, though none of the data collected was at high resolution. These conditions were then optimized, yielding a ~150μm crystal that formed at room temperature in 1.2M K/Na tartrate, 0.2M lithium sulfate and 0.1M Tris pH 7.0 with a starting concentration of protein at 6mg/ml. This crystal diffracted to 3.2 Å with a P6 2 2 space group and unit cell size of 45.33Å x 45.33Å x131.1Å, however, the R_{merge} value and mosaicity were poor, 20% and 1.4 respectively (Fig 2).

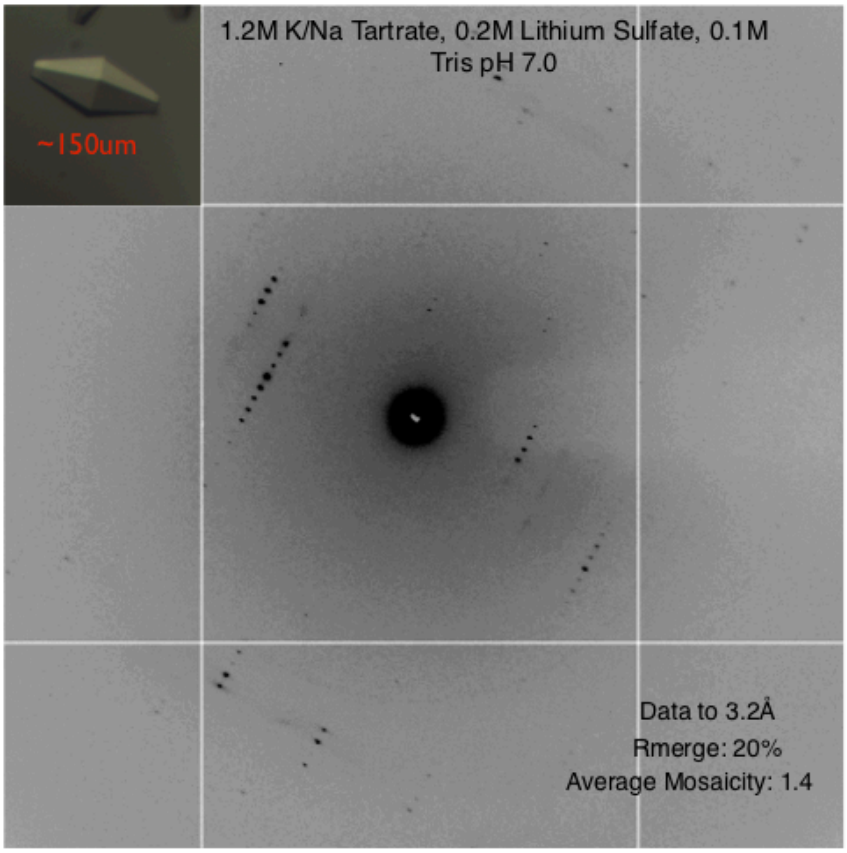

Figure 2. Dimeric CM2 crystal and x-ray diffraction. X-ray diffraction collection image showing protein diffraction out to 3.2 Å. Inset: Image of the crystal with diamond shape morphology.

Because the quality of the crystal was not ideal, I made a number of additional constructs to set up crystal screens (Fig 3). A number of these were small changes to the amino terminus boundary of the construct, CnnCT 1053/1059/164/1066/1068/1071/1073/1077 to the end the protein. Additionally, the monomeric construct CM2 aa1090-1148 was used with the rationale that perhaps the additional amino terminus residues were unstructured and could be trimmed down to the start of the coiled-coil prediction. Furthermore, the constructs aa987-1148 and aa967-1148 were made with the rationale that extending the amino-terminus boundary through the predicted unstructured region (aa987-1148) and through a small region of coiled coil 9aa967-1148) may help with stability and behavior of the crystals. CM2 from the mouse homologue,

CDK5RAP2, and two additional drosophila species, *persimilis* and *grimshawi*, were also cloned, expressed and purified for this purpose. All these protein constructs were set up in crystals screens JCSG Suites I, II, III, IV and Classical Suite I and II. Though numerous of these constructs formed crystals, none were of better quality that the original data set with aa1064-1148, with the exception of the monomeric construct aa1090-1148.

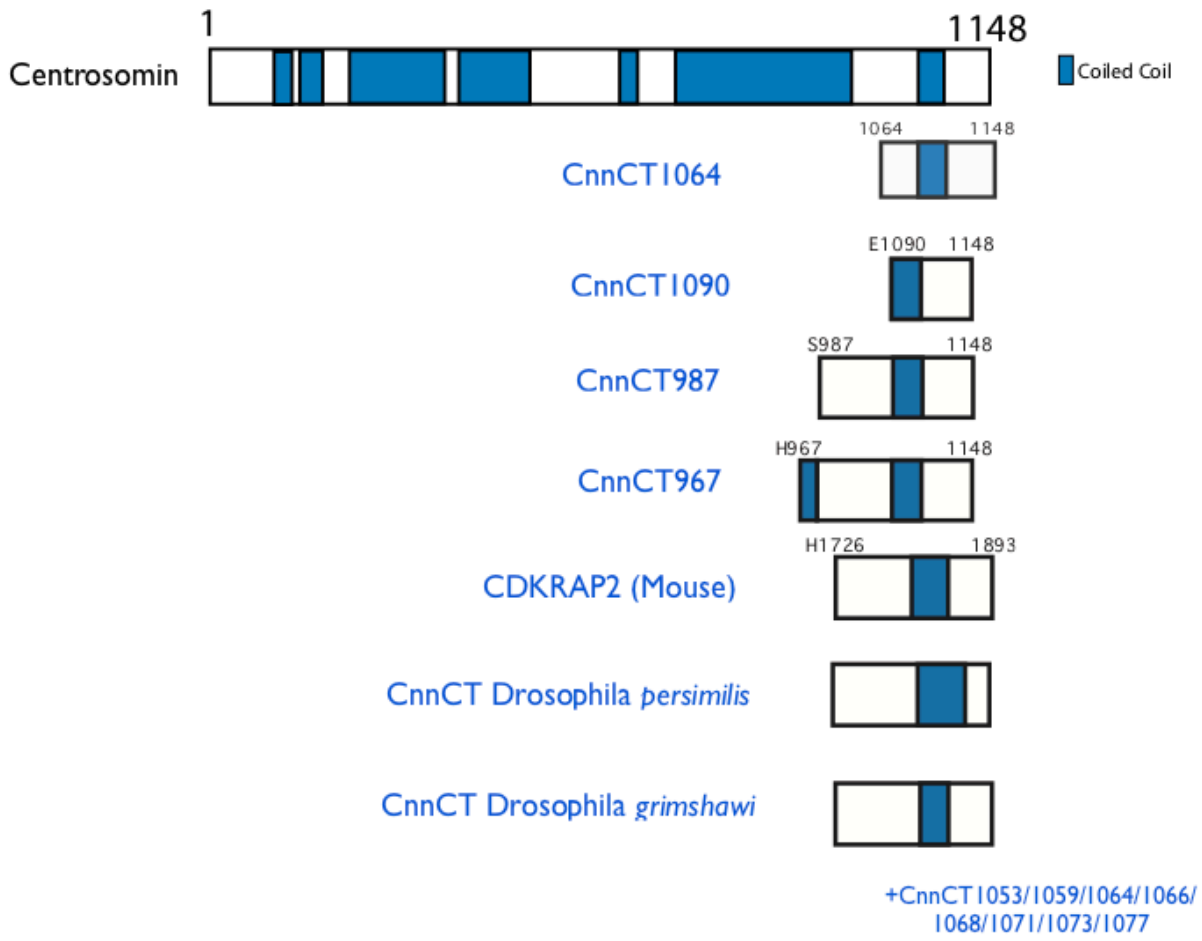

Figure 3. Schematic of the all CM2 constructs made and purified for crystal screening.

Monomeric CM2 formed the highest quality diffraction crystals at room temperature in 0.1M NaCl, 1.6M ammonium sulfate, and 0.1M HEPES pH 7.5 with 3mg/ml protein

concentration. This large rod crystal diffracted out to 2.6 Å with a space group of P6 3 and unit cell size of 79.33Å x79.33Å x 75.52Å (Fig 4). The statistics of this data collection were significantly better with an R_{merge} of 12.3% and a mosaicity of 0.69.

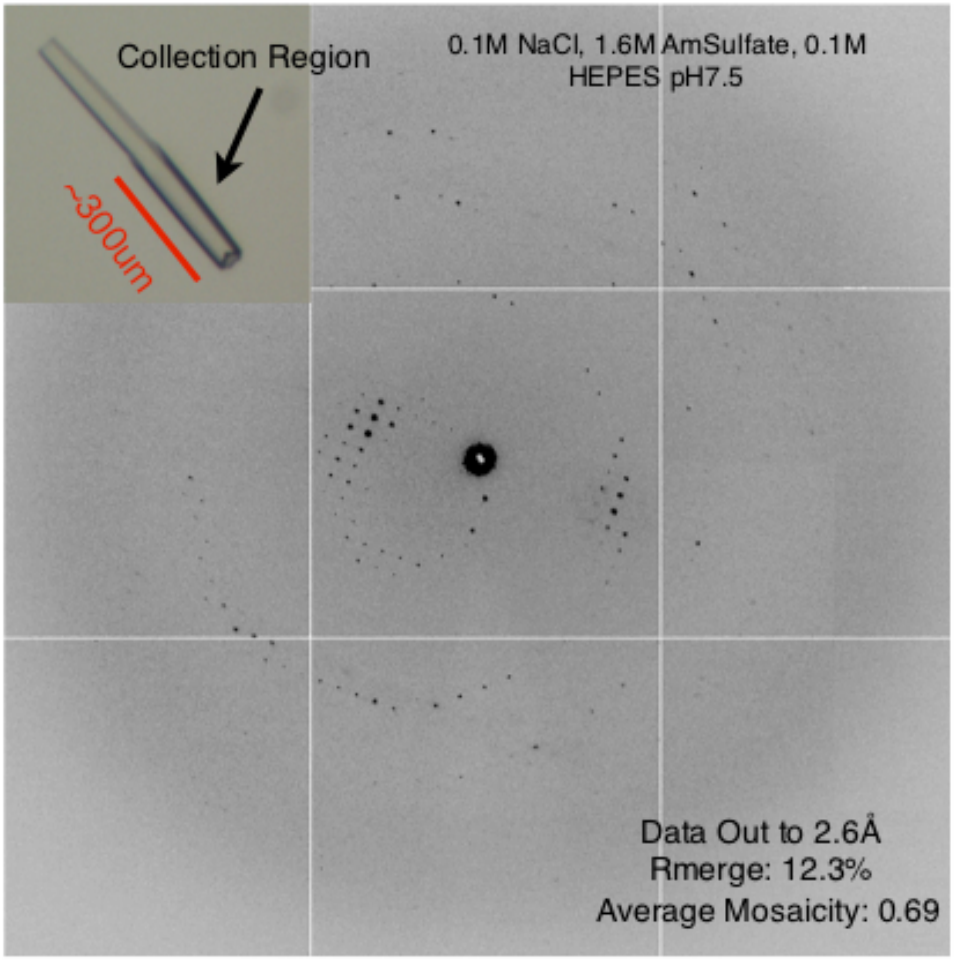

Figure 4. Monomeric CM2 crystal and x-ray diffraction. X-ray diffraction collection image showing protein diffraction out to 2.6 Å. Inset: Image of the large rod crystal.

With this quality of diffraction, I turned towards phasing methods starting with producing selenomethionine labeled protein as this CM2 construct contained two methionines. Despite optimization, crystal trays set with the selenomethionine protein produced much smaller crystals with the largest being around 50 µm, approximately 6x smaller than the native protein crystals. Furthermore, the selenomethionine protein crystals diffracted at best to ~20 Å, with most (~90%)

having even worse diffraction. In an attempt to produce better diffracting crystals, I tried an additive screen and found that the addition of 1,6 diaminohexane changes the morphology from rods to diamonds and yielded very large beautiful crystals of the native protein. I then used this new condition with the selenomethionine protein and was able to produce significantly larger crystals (~200μm). These selenomethionine protein crystals diffracted to 3.25 -5Å, however, after numerous failed attempts at processing and consultation with James Holton these crystals had perfect 50:50 merohedral twinning making them useless for phasing.

From here, I moved onto other phasing methods. Though no homology model of CM2 existed, we reason that a model of a generic coiled-coil could be used as model for molecular replacement. As such James Holton set about, producing ~40,000 generic coiled-coil models for molecular replacement varying the pitch, the super-helical radius, and ect. and both with and without sidechain decoration. Molecular replacements with these models was then preformed using the dimeric CM2 aa1064-1148 data set. None of these models yielded a reliable result in molecular replacement. Given the crystal structure that was published in complex with CnnMD, that none of these models worked makes sense as we expect that even without being bound to CnnMD, CM2 is splayed in a non-canonical coiled-coil conformation.

Additionally, I set about doing heavy metal and sodium bromide soaks with the monomer CM2 protein crystals hopes of collecting anomalous data. However, I found that the soaks caused significant damage or significantly reduced resolution such that no anomalous data was collected on these crystals.

Methods and Materials

Protein Purification

All proteins in this section were expressed using a pET28a vector, either with TEV or PreCission protease cleavage sites. Selenomethionine expression was done using a modified protocol from VanFuyne [2] which was as follows 1mL 1M $MgSO_4$, 330µL 0.2M $CaCl_2$, 1mL 4.2mg/ml $FeSO_4$, 10ml 40% glucose, 100µL 0.5% w/v thiamine, and antibiotics were added to 1L of M9 media pre-warmed to 37ºC. A 10mL overnight culture was then spun down for 2min at 1000xg and re-suspended into M9 media to inoculate the culture. Once the culture reached an OD_{600} of 0.5 amino acids were add: 100mg/L of L-lysine, L-phenylalanine, L-threonine; 50mg/L of L-Isoleucine, L-leucine, L-valine and finally 50mg/L of L-selenomethionine. After addition of amino acids the culture was grown for 30min before addition of 1mM IPTG and allowing expression at normal temperature. Purification than proceeded as normal except for the addition of extra reducing agent, 10mM *b*-mercaptoethanol or 5mM DTT.

All proteins were purified in a similar fashion with lysis using Emulsiflex C3 in 50mM HEPES pH 7.0, 300mM NaCl, 10mM imidazol, and 6mM beta-mercaptoethanol buffer. Lysates were clarified by ultracentrifugation at 35,000xg and the supernatant was incubated with Qiagen NiNTA Superflow resin with gentle agitation for 1.5–2 hours. The resin was washed in batch using 50ml lysis buffer and eluted with a 300mM imidazol buffer. The 6xHIS tagged was cleaved off with 3C protease or TEV. The pooled elution was then further purified by cation exchange chromatography and size chromatography on S75 column (GE).

The exception to this purification protocol was the homologue of CM2 from mouse CDK5RAP2. This protein required a denaturing prep in which the pellet after clearing the lysate was re-suspended in 6M Urea and 50mM HEPES pH 7.0. The protein was then incubated with

Qiagen NiNTA Superflow resin with gentle agitation for 1.5–2 hours. The resin was washed in batch using 50ml lysis buffer and eluted with a 300mM imidazol buffer. The protein was then refolded on the cation exchange column and then size chromatography was carried out.

In all preps, extra final storage buffer without protein was frozen so that buffers in SAXS and crystal trays could be matched.

SAXS Data Collection

Each experiment was collected with a total of 90-min exposure (15 s x 360 frames) using an in-house (Anton Paar SAXSESS mc2, Graz, Austria) SAXS instrument. Fitting of scattering intensity was done using a custom-written software written by Daniel Elnatan in Python2.7 and Fortran (a copy is archived at https://github.com/elifesciences- publications/UCSFsaxs). *Ab initio* modeling was done using DAMMIN in the ATSAS data analysis suite [3].

Crystallization, X-Ray Diffraction Data Collection and Processing

All crystals were grown as hanging drops. Nanoliter pipetting was done by the mosquito (ttplabtech) for initial screens in 96 well format. Heavy metal soaks were done with the heavy metals in the Heavy Atom Screen Pt Individual Reagents and according the accompanying protocol. All diffraction data were collected at beamline 8.3.1 at the Advanced Light Source in Berkeley, CA (at 91.4K and at 1.116Å wavelength, except anomalous data collection). Data was processed using iMosflm [4].

References

1. Feng Z, Caballe A, Wainman A, Johnson S, Haensele AFM, Cottee MA, et al. Structural Basis for Mitotic Centrosome Assembly in Flies. Cell. Elsevier Inc; 2017 Jun 1; 169(6):1078–1083.e13
2. Rambo RP, Tainer JA. Accurate assessment of mass, models and resolution by small-angle scattering. Nature. 2013 Apr 25;496(7446):477-81. doi: 10.1038/nature12070.
3. Franke, D, Petoukhov, MV, Konarev, PV, Panjkovich, A, Tuukkanen, A, Mertens, HDT, Kikhney, AG, Hajizadeh, NR, Franklin, JM, Jeffries, CM and Svergun, DI. ATSAS 2.8: a comprehensive data analysis suite for small-angle scattering from macromolecular solutions. 2017. J. Appl. Cryst. 50, 1212-1225 doi:10.1107/S1600576717007786
4. Battye TGG, Kontogiannis L, Johnson O, Powell HR & Leslie AGW. iMOSFLM: a new graphical interface for diffraction-image processing with MOSFLM. Acta crystallographica. Section D, Biological crystallography 67, 271–281 (Apr. 2011).

Chapter V – Future Work

Chapter II and III report a series of experiments done to characterize the oligomer state, function, and structure of the CM2 domain in centrosomin. From these data a number of conclusions have been drawn regarding CM2's role in driving assembly of the centrosome, however, as in all scientific pursuit, the addition of knowledge propagates more questions.

A number of straightforward questions should be pursued by more thorough characterization of CM2 in complex with PLPMD and calmodulin. Beyond establishing the stoichiometries of these complexes and their affinities, a first pass should be setting crystal trays of these complexes to gain an atomic level structures with X-ray diffraction. For CM2-PLPMD these data would confirm the prediction that PLPMD is a canonical dimeric coiled-coil and give another orthogonal affirmation of the residues involved in complex formation. An X-ray crystal structure of the CM2-calmodulin potentially could illuminate the function of this interaction. For example, a structure may provide confirmation that calmodulin occludes PLPMD or CNNMD binding as proposed in chapter II.

The role of calmodulin in regulating Cnn should also be addressed by trying to disentangle the interactions *in vitro*. Identification of mutations that disrupt calmodulin interaction with CM2 but don't abolish CNNMD or PLPMD binding would be useful in identifying a calmodulin dependent phenotype in cells.

Another approach to understanding the role of calmodulin as well as gaining a more insight into formation and regulation of the CM2 driven matrix, is to perform a more complex *in vitro* reconstitution. Adding in more components, including calmodulin, as well as attaching CM2 to a bead can help explain the growth of the PCM, the protein turnover and pattern in

turnover seen in live cells, as well as the disassembly of the PCM after mitosis. This system can be a platform for understanding a number of unanswered questions. With the current limited knowledge, it is challenging to conceptualize how these small domain interactions occur in the context of proteins ~20x the length. Various truncations, as well as mutations that disrupt dimerization can be tested in this context by characterizing growth, FRAP, or total protein mass.

On a broader note, this work indicates that existence of short motifs, like CM2, in the centrosome that can bind a number of different canonical coiled-coils of divergent primary sequence. The structure of CM2 hints to an open solvent exposed that may be responsible for this promiscuity. It would be interesting to investigate if this type of motif is present in other proteins in the centrosome and if there is a sequence signature that can identify these motifs. While the most convincing evidence would be to preform similar structural and biochemical experiments on other candidates that are highly conserved, these is a large endeavor. An alternative may be to investigate candidates through targeted yeast-two-hybrid assays with short conserved regions containing predicted coiled-coils as bait and assesses the number of bait hits.

Publishing Agreement

It is the policy of the University to encourage the distribution of all theses, dissertations, and manuscripts. Copies of all UCSF theses, dissertations, and manuscripts will be routed to the library via the Graduate Division. The library will make all theses, dissertations, and manuscripts accessible to the public and will preserve these to the best of their abilities, in perpetuity.

Please sign the following statement:

I hereby grant permission to the Graduate Division of the University of California, San Francisco to release copies of my thesis, dissertation, or manuscript to the Campus Library to provide access and preservation, in whole or in part, in perpetuity.

Author Signature

06SEPT2018

Date